AN ABSTRACT OF THE THESIS OF

Minalben B. Shah for the degree of Master of Science in Materials Science presented on August 27, 2003.

Title: Thermodynamics and Kinetics of $Zr_{58.5}Cu_{15.6}Ni_{12.8}Al_{10.3}Nb_{2.8}$ Bulk Metallic Glass Forming Alloy.

Abstract approved:

Redacted for Privacy

9/22/03

Ralf Busch

Among recently found multi-component Zr-based bulk metallic glasses (BMG), $Zr_{58.5}Cu_{15.6}Ni_{12.8}Al_{10.3}Nb_{2.8}$ is characterized by its lower critical cooling rate requirement and absence of beryllium as one of the constituent element which makes its handling more convenient. Its large supercooled liquid regions made possible the study of thermodynamics and kinetics of this alloy. Precise thermal measurements were performed using Differential Scanning Calorimeter (DSC) and Differential Thermal Analysis (DTA). Specific heat capacity measurement in the glass, supercooled liquid and crystalline region were performed with reference to sapphire to evaluate the thermodynamic functions. Enthalpy, entropy and Gibbs free energy difference between supercooled liquid and crystal were calculated as a function of temperature. Smaller Gibbs free energy difference upon undercooling reflects the high glass forming ability of this alloy. Isothermal relaxation and crystallization studies of $Zr_{58.5}Cu_{15.6}Ni_{12.8}Al_{10.3}Nb_{2.8}$ bulk metallic alloy have been performed in the glass transition and the supercooled liquid

region. The temperature range in relaxation experiments is usually lower than T_g due to its low thermal stability with respect to crystallization at higher temperatures. An experimental method of enthalpy relaxation has been developed to study the isothermal relaxation kinetics. The relaxation data obtained for temperatures below the onset of the glass transition temperature was fitted using a stretched exponential function. Results reveal that enthalpy does relax in an Arrhenius fashion. The activation energy of the $Zr_{58.5}Cu_{15.6}Ni_{12.8}Al_{10.3}Nb_{2.8}$ obtained from the Arrhenius fit can be correlated with the activation energy for diffusion of constituent species. Medium sized and small sized atoms are likely to diffuse through collective hopping mechanism. Yet further investigation is required to understand the diffusion mechanism at lower temperatures. Also, the stretching exponents are close to unity, which indicates that the alloy is a rather strong glass former. This is confirmed by Vogel Fulcher Tammann (VFT) fits of the heating rate dependence of the glass transition. The Time Temperature Transformation (TTT) diagram determined close to the glass transition by heating the sample to isothermal temperature being in good agreement with that of the C. C. Hays TTT diagram, which is obtained by cooling the alloy from stable melt. This surprising agreement reveals the stable and homogeneous nature of $Zr_{58.5}Cu_{15.6}Ni_{12.8}Al_{10.3}Nb_{2.8}$ glass forming liquid and its regular nucleation and growth mechanism at any temperatures.

Thermodynamics and Kinetics of $Zr_{58.5}Cu_{15.6}Ni_{12.8}Al_{10.3}Nb_{2.8}$ Bulk Metallic Glass Forming Alloy

by

Minalben B. Shah

A THESIS

submitted to

Oregon State University

in partial fulfillment of
the requirements for the
degree of

Master of Science

Presented August 27, 2003

Commencement June 2004

Master of Science thesis of Minalben B. Shah presented on August 27, 2003.

APPROVED:

Redacted for Privacy

Major Professor, Representing Materials Science

Redacted for Privacy

Coordinator of Material Science Program

Redacted for Privacy

Dean of the Graduate School

I understand that my thesis will become part of the permanent collection of Oregon State University libraries. My signature below authorizes release of my thesis to any reader upon request.

Redacted for Privacy

Minalben B. Shah, Author

ACKNOWLEDGEMENTS

I would like to express my sincere gratitude to Oregon State University, Mechanical Engineering Department to commence this thesis in first instance.

I am greatly obliged to my advisor Prof. Ralf Busch for his stimulating suggestions, constant support and encouragement. I really appreciate his indispensable time, efforts and immense help during research and thesis writing.

Big thanks to my colleagues Ludi Shadowspeaker for his motivating and enthusiastic approach, Tyler Shaw for his support, interest and valuable hints and Isabella Gallino for her constructive comments during DTA calibration and thermodynamic calculations. I am grateful to Manish Bothara, Prashant Wadhwa and Ivan McCracken for their timely assistance.

I would also like to thank Prof. Skip Rochefort for allowing me to use Differential Thermal Analyzer. I would also like to acknowledge Caltech Laboratory for providing samples and National Science Foundation (NSF) for funding this research.

Above all, especially I would like to express my sincere thanks to my husband whose moral support, motivation, understanding and patient love enabled me to complete this work. Lastly, I would like to thank my parents who taught me hard work by setting an example.

TABLE OF CONTENTS

TABLE OF CONTENTS (Continued)

LIST OF FIGURES

LIST OF FIGURES (Continued)

LIST OF FIGURES (Continued)

LIST OF FIGURES (Continued)

LIST OF TABLES

Tables Page

Thermodynamics and Kinetics of $Zr_{58.5}Cu_{15.6}Ni_{12.8}Al_{10.3}Nb_{2.8}$ Bulk Metallic Glass Forming Alloy

1 INTRODUCTION

In today's growing technological era where most metals and alloys are crystalline or polycrystalline in nature, amorphous solids are making their way into this highly developed crystalline world. Lack of repetitive orderly lattice structure or translational symmetry of the amorphous solid is the primary distinguishing feature from that of the crystalline structure. The atoms are arranged in a random fashion as that of liquid and exhibit short-range order. Main advantages of being amorphous in nature are absence of microstructural crystalline defects such as grain boundaries and dislocations.[1] Some examples of amorphous solids include silicates, polymers, rubbers and metallic glasses.

Glasses are different from amorphous solid in a way that they are liquids, which are "frozen" on the time scale of experimental observation and they transform to glass only below its glass transition temperature T_g. Initial work by Klement, Willens and Duwez[2] towards reporting first amorphous Au-Si alloy formed by rapidly quenching to liquid nitrogen temperature, attracted considerable interest among materials scientists in the early 1960's. Invention of ferrous (Fe, Co, Ni) and nonferrous (Pd, La, Mg, Al, Ti and recently Zr) metal-based metallic glasses paved way to fascinating advances in the science of liquid metals. The ability for glass formation lies in the requirement of appropriate cooling rate and wider range of experimental time scale and not in the questionability of forming glass from any kind of material.[3] In the past, very high critical cooling rate was required in the manufacturing of metallic glasses to prevent crystallization. Here, critical cooling rate is defined as the slowest cooling rate required to

form metallic glass. The thickness t of the metallic glass is inversely proportional to the square root of critical cooling rate R_c ($t \propto 1/\sqrt{R_c}$). In case of glass formation where cooling rate requirement was 10^5-10^6 K/s, the sample thickness was limited to micron size because requirement of rapid cooling set restrictions on maximum achievable sample size. One of the possible explanations for size limitation is that during cooling heat can be removed only from the sample surface and heat flow by conduction inside the sample. Further more, materials that are forced into glassy state by using very high cooling rate are not stable against crystallization unless used at very low temperatures.[3] Development of ternary Bulk Metallic Glasses (BMG) in late 1980s reduced this cooling rate requirement to 10^3 K/s.

With advancement in scientific and technological understanding along with manufacturing techniques, it is possible at present to make multicomponent glass forming alloy of centimeter scale thickness with cooling rate of less than 1 K/s.[4] Increased Glass Forming Ability (GFA) is attributed to reduce stability with respect to crystallization. Use of Bulk Metallic Glass (BMG) was limited by its inability to govern technical processes or conventional experimental methods. Requirement of fluxing and special processing techniques are replaced today by conventional metallurgical casting methods. Even today, some of the special processing techniques that are commonly used in preparation of amorphous glasses include Thermal Evaporation, Sputtering, Chemical Vapor Deposition (CVD), Melt Quenching, Melt Spinning, Splat Quenching, Electrolytic Deposition, Irradiation, Solid State Amorphization, Mechanical Alloying and Pressure Induced Amorphization.

1.1 Objective

The objective of this research is to enhance the basic thermodynamic understanding by carrying out specific heat capacity measurements on $Zr_{58.5}Cu_{15.6}Ni_{12.8}Al_{10.3}Nb_{2.8}$ Bulk Metallic Glass (BMG) and deriving various thermodynamic functions from it. Also, to contribute to ongoing research of kinetic phenomenon by performing isothermal enthalpy relaxation studies of $Zr_{58.5}Cu_{15.6}Ni_{12.8}Al_{10.3}Nb_{2.8}$ in the glass transition and supercooled liquid region and developing an experimental method of enthalpy measurement as a function of time.

1.2 Area of Research

Modern bulk metallic multi-component alloys show excellent glass-forming ability.[5-7] Recently found Vitreloy with a composition of $Zr_{58.5}Cu_{15.6}Ni_{12.8}Al_{10.3}Nb_{2.8}$ (at%) is a revision in a series of Vitreloy $Zr_{41.2}Ti_{13.8}Cu_{12.5}Ni_{10}Be_{22.5}$, $Zr_{46.75}Ti_{8.8}Cu_{7.5}Ni_{10}Be_{27.5}$, $Zr_{52.5}Ti_5Cu_{17.9}Ni_{14.6}Al_{10}$ and $Zr_{57}Cu_{15.4}Ni_{12.6}Al_{10}Nb_5$. This alloy has improved glass forming ability compared to neighboring compositions in the Zr-Nb-Cu-Ni-Al alloy with small changes in the Zr-Nb and Cu-Ni-Al ratios.[8] It is possible to make centimeter scale castings of this alloy even with an arc melter. This alloy doesn't contain beryllium and can be processed by the critical cooling rate of less than 10 K/s (as low as 1.75 K/s) [9]. Both these are important factors that help in predicting large-scale processability of this alloy.

In this research efforts have been made to determine the thermodynamic properties of $Zr_{58.5}Cu_{15.6}Ni_{12.8}Al_{10.3}Nb_{2.8}$ in the undercooled liquid and the amorphous phase using Differential Scanning Calorimetry (DSC) and Differential Thermal Analysis (DTA).

Experiments have been carried out to measure specific heat and heat of transformation close to glass transition temperature and crystallization temperature. Thermodynamic functions are calculated based on the obtained experimental results. Along with thermodynamics it is also important to study kinetics in the proximity of glass transition region. Importance of relaxation process lies in the fact that thorough understanding of this phenomenon is indispensable for explaining glass transition behavior. Most of the research till date focused on understanding the relaxation behavior of bulk metallic glass through viscosity relaxation.[10-13] In this research attempt has been made to gain some insight into kinetic relaxation phenomenon by studying enthalpy relaxation in the glass transition region. Also, in the area of bulk metallic glasses where fluid behavior is well described in high temperature region, thorough understanding still lacks in delineating fluid behavior in the glass transition region. Behavior in glass transition range is studied in a variety of relaxation experiments like stress relaxation, volume relaxation, creep relaxation and dielectric relaxation. In all cases, relaxation in the vicinity of Tg is not described by a single relaxation time. Rather distributions of relaxation times are required to represent experimental data.[14] Enthalpy change near glass transition temperature is calculated using isothermal experimental measurements. Along with relaxation, crystallization behavior is determined in the entire supercooled liquid region.

1.3 Scope of Work

1.3.1 Thermodynamic Study

- Specific heat capacity c_p measurements on $Zr_{58.5}Cu_{15.6}Ni_{12.8}Al_{10.3}Nb_{2.8}$ were performed using sapphire as a standard in the amorphous region, supercooled liquid region and crystallization region with DSC machine.
- Based on the specific heat capacity data, thermodynamic functions [e.g. Enthalpy (ΔH), Entropy (ΔS) and Gibbs free energy (ΔG)] were calculated from liquidus temperature to temperature below the glass transition. Also, from the DSC and DTA plots, heat of crystallization (ΔH_x) and heat of fusion (ΔH_f) were determined.

1.3.2 Kinetic Study

- Heating rate kinetics of $Zr_{58.5}Cu_{15.6}Ni_{12.8}Al_{10.3}Nb_{2.8}$ were studied using DSC at different heating rates between 8.33×10^{-3} to 3.33 K/s.
- Fragility parameter D* and Vogel Fulcher Tammann (VFT) temperature T_0 were calculated by fitting the glass transition data to VFT type equation on a plot of relaxation time as a function of inverse temperature.
- Isothermal DSC experiments on $Zr_{58.5}Cu_{15.6}Ni_{12.8}Al_{10.3}Nb_{2.8}$ were carried out at constant heating rate near the glass transition and supercooled liquid region.
- Enthalpy relaxation time (τ) and stretching exponent (β) were calculated by fitting the data to stretched exponential function for isothermal annealing below T_g.
- Activation energy Q and pre-exponential constant τ_0 were derived by fitting the enthalpy relaxation data with the Arrhenius equation on a plot of relaxation time (τ)

as a function of isothermal temperature (T). These parameters were then compared with results obtained from heating rate experiments.

- Time Temperature Transformation diagram was constructed from isothermal crystallization experiment.

2 THEORY AND LITERATURE REVIEW

2.1 Properties of Bulk Metallic Glass

It is important to study mechanical properties of Bulk Metallic Glass (BMG) in order to investigate its applications as an engineering material. Bulk metallic glasses have very high yield strength and elastic limit. They do not exhibit strain hardening, strain softening or thermal softening.[4] Ferrous metal-based bulk metallic glasses demonstrate excellent soft magnetic properties characterized by low coercive force and high permeability. Zr-based BMG exhibits unique combination of mechanical properties. It has high wear resistance, high corrosion-resistance and low coefficient of thermal expansion. Furthermore, the material exhibits excellent oxidation-resistance. Commercial applications can utilize its high strength to weight ratio, high bending strength, high hardness, high fracture toughness, high impact fracture energy, high fatigue strength, good castability and good machinability.[15] Bulk metallic glass based composites have been manufactured recently with improved plasticity and which will enhance its application in engineering arenas. Homogeneous dispersion of nanoscale particles into Zr-based bulk amorphous alloys was found to improve tensile strength without detrimental effect to ductility. [4] Formation and motion of localized shear bands at high strain rates have major influence on the deformation property of bulk metallic glasses.[16] Highly disordered structure of bulk metallic glasses is also reasonably resistant to radiation damage.[14]

2.2 Applications of Bulk Metallic Glass

Above mentioned properties of BMG find useful technical applications in the field of structural materials, magnetic materials, acoustic materials, optical machinery materials, sporting good materials (e.g. golf club, baseball bats, bicycle spokes) and electrode materials.[17] Recently, BMG are also utilized in manufacturing transformer cores, capacitors and as magnetic sensors in security devices. Its high permeability combined with high hardness makes it a well-suited candidate for tape recorder heads.[14] It can also be used in the manufacturing of razor blades due to its high corrosion resistance, hardness and elastic limit. Its immunity to outside environment makes it a useful candidate for protective surface coatings. Upcoming field of application using bulk metallic glass include manufacturing of cell-phone cases and watch cases. Extensive research is going on in defense area to explore its use in missiles and armors. It can also be used in aircraft components. One of the latest researches by NASA in collaboration with Caltech, USA and University of Zurich, Switzerland explored the use of Zr-based bulk metallic glass in catching pieces of solar wind. Ability of BMG to dissolve ions evenly and release it layer-by-layer when etched using some sophisticated acid-etching technique was the principal basis for this application.[18]

2.3 Definition of Thermodynamic Properties

Specific Heat (C_P) [19] is the quantity of heat required to raise the temperature of the substance by one degree Kelvin at constant pressure. It is symbolized by C_p.

$$C_p = \left(\frac{\partial H}{\partial T}\right)_P \quad (1)$$

where, H is the enthalpy and T is the temperature of substance at constant pressure.

Enthalpy (H) [19] is a measure of heat content of the system and is expressed by the equation H = E + PV where, E is the internal energy of the system, P the pressure and V the volume. Internal energy E is the sum of kinetic energy and potential energy of the system. Kinetic energy arises due to vibration in solid or liquids or from translational and rotational energies of the atoms and molecules within a liquid or gas. Potential energy arises from the interactions, or bonds, between the atoms within the system. Variation of enthalpy with temperature is calculated by knowledge of specific heat

$$\Delta H = \int_{T_1}^{T_2} C_p dT \quad (2)$$

Entropy (S) [19] is the measure of the randomness of the system. In terms of statistical thermodynamics, entropy is related to Boltzmann constant and is given by

$$S = k \ln \omega \quad (3)$$

where, k is Boltzmann constant and ω is a measure of randomness. Two main contributions of entropy are thermal contribution S_{th} and configurational contribution S_{config}. In case of thermal entropy, ω is the number of ways in which the thermal energy of the solid can be divided among the atoms and in configurational entropy ω is the number of different ways of arranging atoms in the solution. The entropy change in a reversible process is defined as

$$dS = \frac{dQ}{T} \qquad \rightarrow \qquad \Delta S = \int_{T_2}^{T_1} \frac{C_p}{T} dT \tag{4}$$

At constant enthalpy, entropy always tends to increase. In addition, according to the third law of thermodynamics the entropy of a pure, perfect crystal is zero at absolute zero (0 K).

Gibbs Free Energy (G) [19] determines the relative stability of the system and is given by G = H – TS, where H is enthalpy, T the absolute temperature and S the entropy of the system. A system is considered to be in stable equilibrium if it has the lowest possible value of the Gibbs free energy ($\Delta G = 0$). Difference in Gibbs free energy, which is important during the phase transformation between two phases at certain temperature, is given by

$$\Delta G = \Delta H - T\Delta S \tag{5}$$

2.4 Importance of the Glass Transition (T_g)

The glass transition temperature T_g is generally defined as the point of inflection of the rising C_p.[14] It is a kinetic phenomenon caused by the inability of the liquid structure to equilibrate on an experimental timescale at sufficiently low temperatures. Glass transition is not a first or second order phase transformation but it is a kinetic event, which depends upon the crossing of an experimental time scale and time scale for molecular rearrangements.[20] The range of temperature over which transformation takes place is called "transformation range" and the center of the transformation range can be used to define the glass transition temperature T_g.[3] It depends on the heating and cooling rate. In

addition to the position of T_g, the width of the transformation region also depends on the cooling rate. The glass transition region usually becomes narrower by lowering the cooling rate. The reason behind this is the molecular relaxation time (τ), which is a function of temperature. For example, relaxation time of metallic glass is about 10^{-12} sec at melting temperature T_m, 10^3 sec at T_g and 10^{13} sec (317098 years) far below T_g. The relaxation time is compatible to the time scale of experiment at T_g but below T_g, τ becomes so large that molecules cannot rearrange to equilibrium state within experimental time period. This slowdown of kinetics near glass transition is related to change in viscosity. So, in first approximation viscosity is proportional to relaxation time ($\eta \propto \tau$).[21] In general, glass transition temperature increases by alloying metallic elements having strong attraction and that are refractory.

2.5 Glass Forming Ability in Multicomponent Alloys

Bulk metallic glasses are dense liquids with small free volumes and very high viscosities compared to pure metals and previously known alloys.[22] In bulk metallic glass forming alloys where three to five metallic elements are alloyed together, the liquid enthalpy of mixing is lowered resulting in a lower melting point alloy.[4] Also, compositions are selected in proximity of deep eutectic. Chen[23] proposed that the destabilization of crystalline mixture near the eutectic composition determines the stability and the ease of glass formation. At low temperature glass formation is easy due to high viscosity and low rate of structural relaxation but at high temperatures glass formation is governed by cooling rate requirement of particular material. Many factors influence the glass forming

ability of an alloy. The cooling rate depends on the thermo physical and kinetic properties, which themselves are a function of chemical composition.

It is also important to understand the frustration principle[4] of crystallization process, which contributes in improving glass forming ability of multicomponent alloy. When different atomic species are put together the resulting crystalline alloy suffer with the chemical disorder. This chemical disorder is associated with the local atomic strains arising from the atomic size difference as well as difference in valence electron configuration of the constituent species. Also, going from one element to five-element system, probability of forming new crystal structure and a chance of getting periodically ordered structure progressively diminishes.

Another factor predicted by Turnbull[24] that is considered to be actively participating in improving glass-forming ability is reduced glass transition temperature T_{rg}. It is a ratio of the glass transition temperature T_g to the liquidus or melting temperature T_m of an alloy. According to him, as the ratio is increased from 0.5 to 0.66 i.e. as T_g gets closer to T_m, the homogeneous nucleation of crystals in the undercooled liquid become sluggish on laboratory time scale and process of crystallization is suppressed. Also, in the case where the viscosity of the liquid near T_m is very high it is in agreement with the basic criteria that liquid with high glass forming ability should have a relatively high viscosity near the melting point. As a result glass formation is most probable near eutectic where the liquidus temperature has a minimum.

Three empirical rules, [17] that predict high glass forming ability of amorphous multi-component systems are based on

- systems consisting of more than three elements
- significant difference in atomic size ratios above about 12% among the three main constituent elements and
- negative heat of mixing among the three main constituent elements.

Alloys that satisfy above three empirical rules can form supercooled liquid with a higher degree of dense randomly packed atomic configurations, new local atomic configurations and long-range homogeneous atomic configurations which has high solid/liquid interfacial energy and hence is favorable for suppressing nucleation of a crystalline phase.

Recently produced Zr-based bulk metallic glass by Johnson and Peker[25] require low cooling rates and are stable above the calorimetric glass transition temperature on experimentally accessible time scale that allows detailed investigation of glass transition and supercooled liquid region. According to Inoue,[26] the wider the Supercooled Liquid Region or SLR widths between the glass transition temperature T_g and the crystallization temperature T_x of the bulk metallic glass, better is the glass forming ability and easier is the application of the new processes.

Recent study on binary metallic glass by Lee et. al.[27] showed that smaller size atom have more diffusivity and more configurational randomness compared to the larger atom. They also found that glass-forming ability increases with packing fraction in the liquid state because densely packed material requires more time to rearrange and crystallize.

2.6 Importance of Crystallization Theory in Glass Formation

According to the classical theory of homogeneous nucleation,[28] the rate of crystal nucleation and growth depends on a kinetic factor that is directly related to the rate of structural relaxation, which also governs the glass transition. Heterogeneous crystallization on undercooling starts mainly at the site of foreign particles or at the container wall. As it is difficult to control these extrinsic factors experimentally, most of the theory is based on intrinsic process of homogeneous nucleation. According to this theory small crystalline nuclei are continuously formed in the supercooled liquid. The growth of these nuclei to macroscopic size is impeded by the presence of activation energy barrier. Here, the activation energy barrier results from a positive surface energy. Only those droplets, which are larger than critical size, contribute in crystal growth. The rate at which nuclei reaches its critical size is considered as the rate of homogeneous nucleation, I. Turnbull[29] theory of nucleation discussed that in order to form the glass from pure metals, the latent heat of fusion, surface tension of the crystal-liquid interface as well as the viscosity as a function of temperature should be known. Later on Uhlmann[30] gave the theory that includes the growth rate of critical nucleus. But none of the previous theories actually described the chemical decomposition of liquid that is required for the formation of stable crystalline phases. Almost all of the existing theories of crystal nucleation and growth are limited by calculating kinetic factor for finding out minimum cooling rate in glass formation.

2.7 Relaxation Kinetics

It is important to clarify temperature regions of interest in discussion of relaxation phenomenon in glass forming alloys. Fig. 1[14, 20] shows schematically the variation of specific volume of crystal, liquid and glass as a function of temperature. On cooling the liquid from high temperatures, there is a discontinuous change in volume when it undergoes crystallization. If the liquid volume decreases with the same rate as above the melting point without crystallization, it is termed as a supercooled or undercooled liquid. As supercooled liquid is cooled to lower temperatures, its viscosity increases and it exhibits solid like behavior. The time scale of molecular rearrangement become so large compared to the experimental observation that the structure is frozen for practical purposes. This frozen structure is called glass and the temperature of this transition from supercooled liquid to glass is called glass transition temperature T_g. During cooling the metastable equilibrium should exist above the transformation range and in the transformation range and below it at least the vibrational degree of freedom should be in equilibrium at any time. But, nevertheless in this range material falls out of the metastable equilibrium of the supercooled liquid since configurational rearrangements are frozen in. The configuration of glass changes to equilibrium structure on holding the glass isothermally in the glass transition region and is considered as relaxation phenomenon. According to Li et.al.[31] structural relaxation phenomenon is described as decrease in the free energy due to rearrangement of atoms in a material upon annealing. Understanding of flow behavior of viscous liquid near glass transition region gives

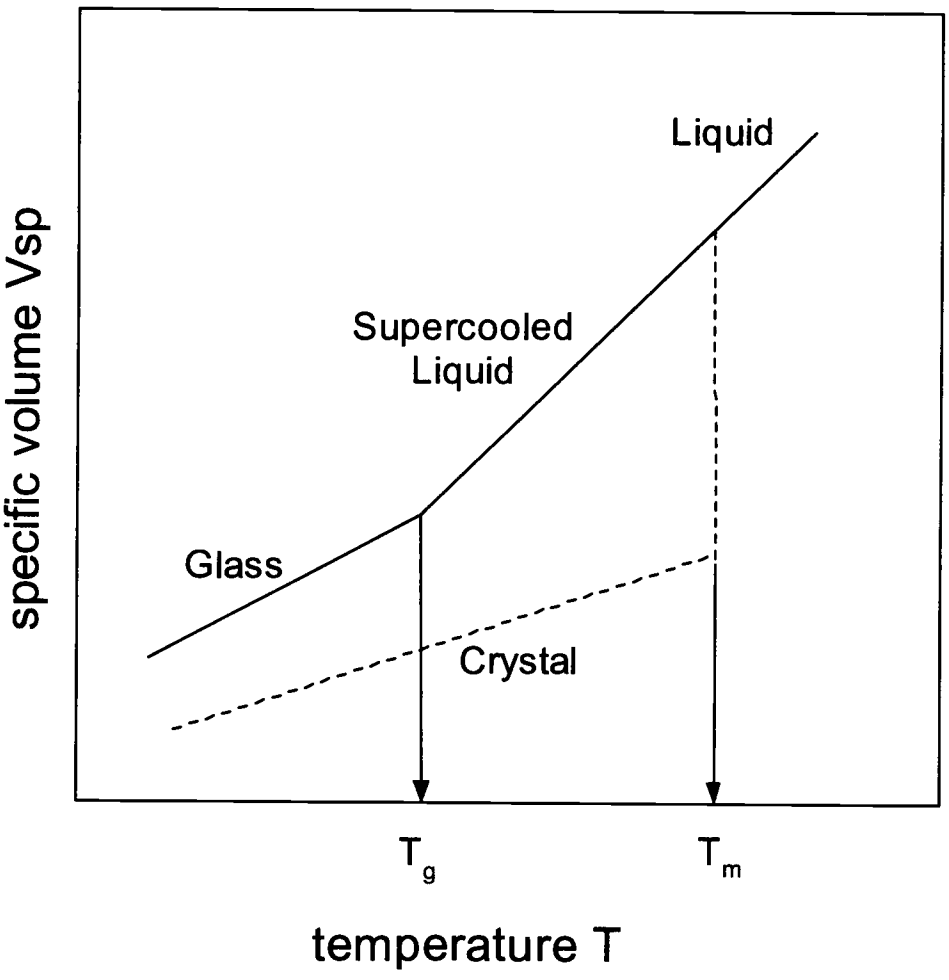

Figure 1 Schematic of the specific volume as a function of temperature for a liquid, which forms both glass and crystal. Formation of glass or crystal depends on cooling rate. T_g designates glass transition temperature and T_m melting temperature.

insight into the relaxation phenomenon. Absolute rate model and free volume model describes the glass transition as a kinetic phenomenon while excess entropy model contradicts it by claiming its origin in thermodynamics.[14]

2.7.1 Absolute Rate Model

According to Absolute Rate Model[14] viscosity is viewed as a rate process and it provides direct description of the stress dependence of flow. In the small stress range, the model predicts Arrhenian temperature dependence for the viscosity (η)

$$\eta \approx \eta_o \exp(\Delta E/kT) \tag{6}$$

2.7.2 Free Volume Model

One of the important structural characteristics of bulk metallic glass is atomic scale open-volume or free volume, which largely affects physical and mechanical properties of alloy. Free volume can be thought of as empty space around the atoms. According to Cohen and Turnbull free volume theory[32], which describes flow behavior, "molecular transport occurs by the movement of molecules into voids, with a size greater than some critical value formed by the redistribution of the free volume." So, the surplus volume in one part of the liquid becomes available in another part without requiring appreciable activation energy compared to k_BT. Where, k_B is the Boltzmann constant and T temperature. Accordingly, slow molecular movement in high viscosity region is attributed to shortage of free volume rather than presence of energy barrier. In case of metallic glasses where atomic arrangement is configurationally frozen, they possess excess free energy that is

associated with frozen-in structural disorder e.g. free volume. The viscosity can be expressed as,[33]

$$\eta = \eta_{\circ} \exp\left(\frac{b\upsilon_m}{\upsilon_f}\right) \tag{7}$$

in which, υ_f is the average free volume per atom and $b\upsilon_m$ is a critical volume for flow.[3,34] Free volume's temperature dependence is given by linear relation $\upsilon_f = \upsilon_m \alpha_f (T - T_{\circ})$, which yields the Vogel Fulcher Tammann (VFT) equation

$$\eta = \eta_{\circ} \exp\left(\frac{b}{\alpha_f (T - T_{\circ})}\right) \tag{8}$$

here, α_f is a measure of the increase in free volume with temperature and according to Williams et.al.,[35] it can be approximated by the difference in thermal expansion coefficients between the liquid and the glass

$$\alpha_f = \alpha_{liq} - \alpha_{glass} \tag{9}$$

Liquid can be classified according to its fragility by replacing $b/\alpha_f T_{\circ}$ with dimensionless parameter D in the above VFT equation.

In addition, Suh and Dauskardt's[36] work suggested that the variation of relaxation time (τ) is associated with reduction in free volume on annealing metallic glass below the glass transition temperature. The same theory can be applied to enthalpy relaxation because it also includes volume.

2.7.3 Excess Entropy Model

According to Kauzmann's excess entropy theory,[37] excess entropy of good glass former near metastable supercooled liquid relative to the same crystalline material extrapolates to zero at temperature T_2 which is very close to the glass transition temperature. This vanishing excess entropy at temperature T_2 is in good agreement with the VFT temperature T_0 at which viscosity becomes infinite as pointed out by Gibbs and Adams.[38] Increasing relaxation time and viscosity in the supercooled liquid by reduction in configurational entropy is given by excess entropy theory of Gibbs and his co-workers.[38,39] Viscosity is expressed as

$$\eta = \eta_0 \cdot \exp\,(C/T \cdot S_c) \qquad (10)$$

in which, S_c is the configurational entropy of the liquid and C is an approximate constant and represents the free enthalpy barrier to cooperative rearrangement.

2.8 Dense Random Packing

Computer model of dense random packing[3] of hard spheres for structure of pure liquid and amorphous metal shows prevalence of Icosahedral (a polyhedron having 20 faces) structure and not crystalline one. Presence of this structure is evident by comparing ordering of bond, nearest neighbor distance and its bond orientation with that of the ideal icosahedron. Nelson[40] correlated this dense packing with the kinetic relaxation and free volume concept. According to him kinetic barrier arises only if the packing is sufficiently dense and there is enough repulsive forces between spheres. If any large fluctuation in the local volume occurs then atom can move freely and kinetic barrier vanishes. At the same

time, there is also presence of energy barrier, which inhibits formation of spontaneous crystalline nuclei, and favors short range ordering.

2.9 Viscosity and Kinetic Relaxation

Dramatic increase of shear viscosity on approaching the glass transition implies a slowing down of shear stress relaxation. On a molecular scale, increase of viscosity is related to reduction in atomic motion. According to Stokes-Einstein relation viscosity is inversely related to diffusivity as per following equation [3]

$$D = k_B T/3\eta\pi a \tag{11}$$

Decrease in diffusivity further leads to characteristic reduction in atomic rearrangements and structural relaxation. Time scale splits in the relaxation spectrum due to slowing down of diffusive atomic motion or due to reduction in shear stress relaxation. Also, the slowdown in shear stress relaxation is contrasted by the increase in vibrational degree of freedom. With decrease in temperature the discrepancy between the fast and slow relaxation mode increases. Furthermore, slow relaxation cannot be described by a single relaxation time and it does not follow the simple exponential relation. Among several empirical expressions for relaxation, Kohlrausch-Williams-Watts (KWW) [41,42] fits the experimental data well. The relaxation function is given by

$$\Phi(t) = \exp[-(t/\tau_0)^{\beta}] \tag{12}$$

where, t = time (sec), τ_0 = average relaxation time (sec), β = stretching exponent

Relaxation function follows time-temperature scaling principle and the relaxation function measured at different temperatures fall on a single master curve if time is scaled

appropriately with average relaxation time $\tau_0(T)$. Stretching exponent β in above equation is independent of temperature and may differ for different relaxing quantities even in the same material. It is very complicated to measure viscosity curve below the glass transition temperature due to the slowness of structural relaxation. A relaxation phenomenon, which is responsible for local molecular rearrangement below the glass transition temperature, is termed as "Secondary Relaxation". [43] It is very interesting to understand the effect of temperature on the viscosity and relaxation time of supercooled glass forming liquid. For strong liquids like quartz, the viscosity follows the Arrhenius trend with high but constant activation energy. These liquids are characterized by the absence of configurational specific heat. For most of the bulk metallic glass forming liquids strong deviation from Arrhenius trend is described by the VFT formula. The activation energy is very high between the melting point and T_g but near T_g it saturates and temperature dependence again become Arrhenius like. This increase in activation energy is sometime connected with the structural change that is evident by its configurational specific heat. These structural changes can be characterized by the formation of molecular clusters of increasing size, which cooperate in the shear stress relaxation process and is known as cooperativity of molecular motion.[44]

The most recent formulation of the VFT relation describes equilibrium viscosity data in the supercooled liquid and is expressed as

$$\eta = \eta_0 \cdot \exp\left[\frac{D^* \cdot T_0}{T - T_0}\right] \tag{13}$$

here, D^*[45] is the fragility parameter or fragility of the liquid and T_0 is the VFT temperature where the barriers with respect to flow would go to infinity. D^* is of the order of 100 for strongest glass former e.g. SiO_2 and yields value as low as 2 for fragile liquids. Strong glass formers are characterized by very high equilibrium melt viscosities, VFT temperature far below the glass transition temperature and follow Arrhenius behavior in supercooled melt. Fragile liquids have low melt viscosities, VFT temperature close to the glass transition and shows more abrupt change in the kinetics close to the glass transition. The value of η_0 can be calculated according to the relation

$$\eta_0 = N_A \cdot h/V \tag{14}$$

in which, N_A represents Avogadro's constant, h Planck's constant and V the molecular volume.[46]

The relaxation process of equilibrium viscosity in the glass transition region is observed to follow stretched exponential function[47] and does not proceed exponentially. The stretched exponential relaxation function is given by

$$\eta(t) = \eta_a + \eta_{eq-a} \cdot (1 - e^{-(t/\tau_s)^\beta}) \tag{15}$$

here, τ_s is an average shear flow relaxation time, β a stretching exponent, t the time and η_a the viscosity of amorphous alloy before relaxation and η_{eq-a} is the total viscosity change during relaxation from the amorphous state into the equilibrium state.

Recent experiments on multicomponent glass forming liquids help understand the structure of bulk metallic glasses.[10] According to these findings small density difference between solid and liquid state indicates small free volume in the liquid at melting and

upon undercooling. Small entropy of fusion of bulk metallic glass forming liquid is suggestive of presence of short-range chemical order that can lead to clustering or phase separation. In addition decrease in thermal and electrical conductivity is indicative of localized electrons as a result of directional bonds. All these findings show that bulk metallic glass forming liquid is more rigid with respect to shear flow and thus a strong glass former.

2.10 TTT Diagram

As the amorphous undercooled metallic liquid is in a metastable state, it crystallizes with proper combination of temperature and time. In isothermal experiments, the Time Temperature Transformation (TTT) diagram provides the time scale for crystallization at constant temperatures. The most characteristic feature of this diagram is a typical "C" or nose shape curve. The C shape is the result of the competition between the increasing driving force for crystallization and the slowing of kinetics (effective diffusivity) of the atoms.[19] It usually represents the onset (1%), intermediate (~50%) and end (99%) time of crystallization as a function of temperature. The nose of the TTT diagram corresponds to minimum amount of time required to initiate crystallization at any undercooling. At nose, the onset time of crystallization does not decrease with decreasing temperature but increases due to the slowdown of kinetics of the undercooled melt.[48] It is possible to estimate the critical cooling rate of the alloy from the position of the nose in the TTT diagram.[4] Materials capability to have high glass forming ability is revealed by shifting of the nose to right hand side or to longer time scale for crystallization when cooled from

liquidus temperature to glass transition temperature. Time scale for crystallization ranges from hundreds of microseconds to milliseconds at the nose of the nucleation curve for initial metallic alloys. Today with the highly stable supercooled liquid region, the minimum crystallization time is increased to hundreds of seconds for BMG liquids. Schematic of time-temperature transformation diagram is shown in Fig. 2.

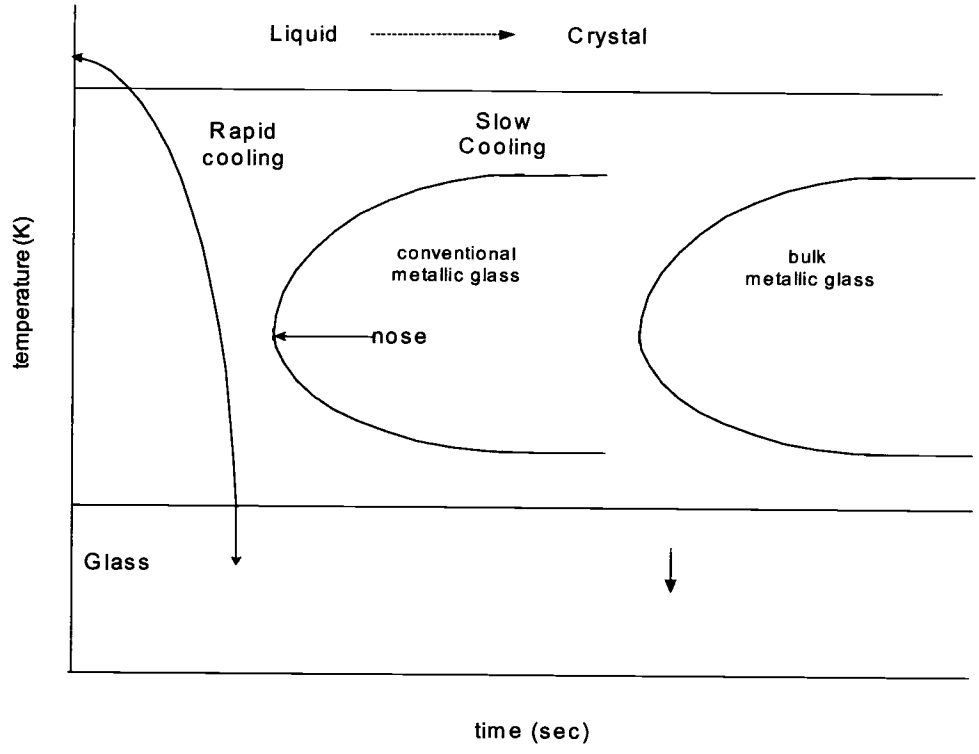

Figure 2 Schematic of Time-Temperature Transformation (TTT) diagram. The curves with the arrow indicate cooling. A rapid cooling result in glass when nose of the TTT diagram is bypassed otherwise on slow cooling crystallization is observed.
(Ref: "Bulk Glass-Forming Metallic Alloys" from W.L Johnson).

3 EXPERIMENTAL METHODS

3.1 Sample Preparation

The specimens used for DSC and DTA analysis were cut from as prepared strip of $Zr_{58.5}Cu_{15.6}Ni_{12.8}Al_{10.3}Nb_{2.8}$ made up of highly pure metals. The purpose of using very high purity metal is to avoid crystallization via heterogeneous nucleation of foreign particles. As the composition of $Zr_{58.5}Cu_{15.6}Ni_{12.8}Al_{10.3}Nb_{2.8}$ can be vitrified with critical cooling rate of as low as 1.75 K/s, [9] it is also possible to manufacture it with conventional arc melting and water-cooled copper boat technique.

3.1.1 Arc Melting System

In our laboratory arc melter, highly pure metals 58.5at% Zr (99.9%), 15.6at% Cu (99.999%), 12.8at% Ni (99.995%), 10.3at% Al (99.999%) and 2.8at% Nb (99.96%) were put together on a circular water-cooled copper hearth to make spherical master alloy (typically 10grams) as shown in Fig. 3. A picture of the laboratory arc melting system is shown in Fig. 4. The system was cleaned by reducing base pressure to 10^{-3} mbar using rotary vane pump and melting Ti-getters. The metals were then melted in an ultrahigh purity (99.999%) argon atmosphere. The arc was ignited when a tungsten rod that acts as a cathode, strikes the copper anode at sufficient DC current of 120-140 amp for melting constituent elements. To ensure homogeneity, each sample was melted three times by flipping it after each melting process.

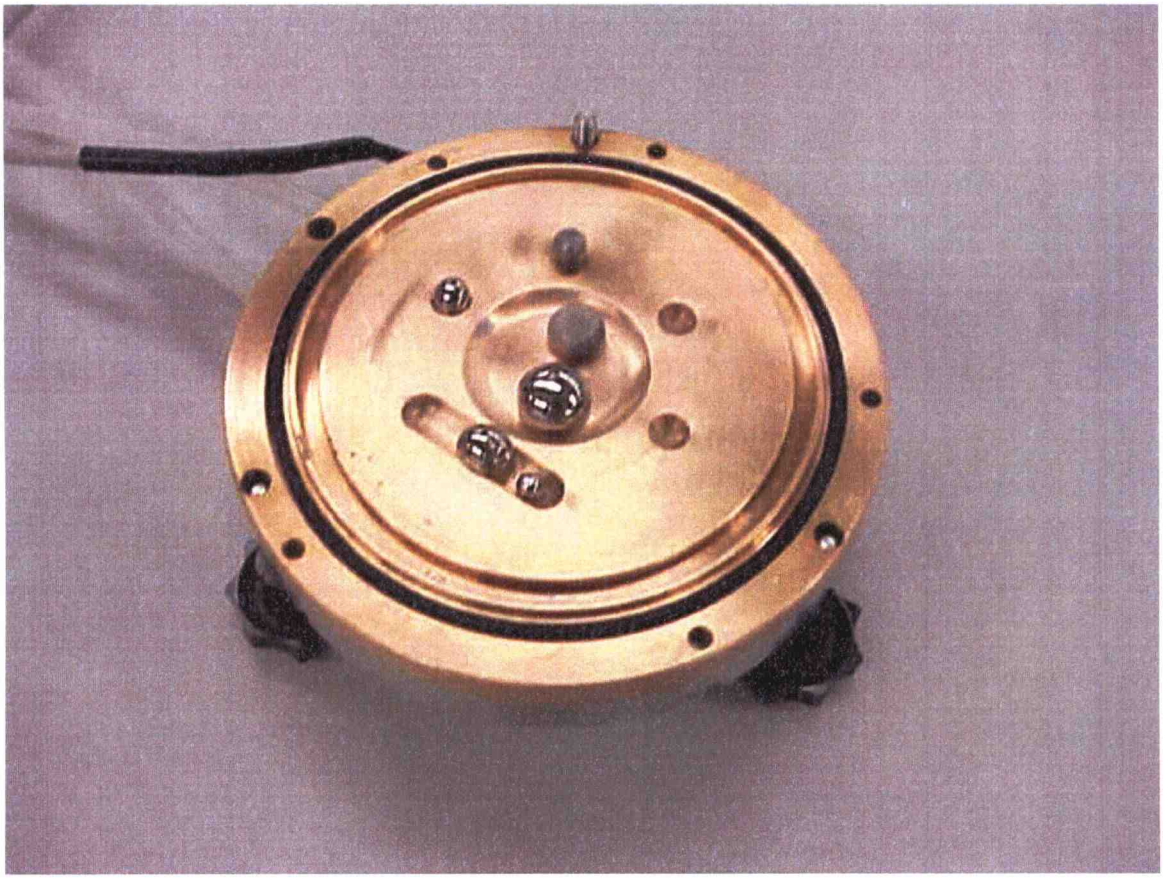

Figure 3 Water-cooled copper hearth for holding sample and Ti getterer in Arc Melter.

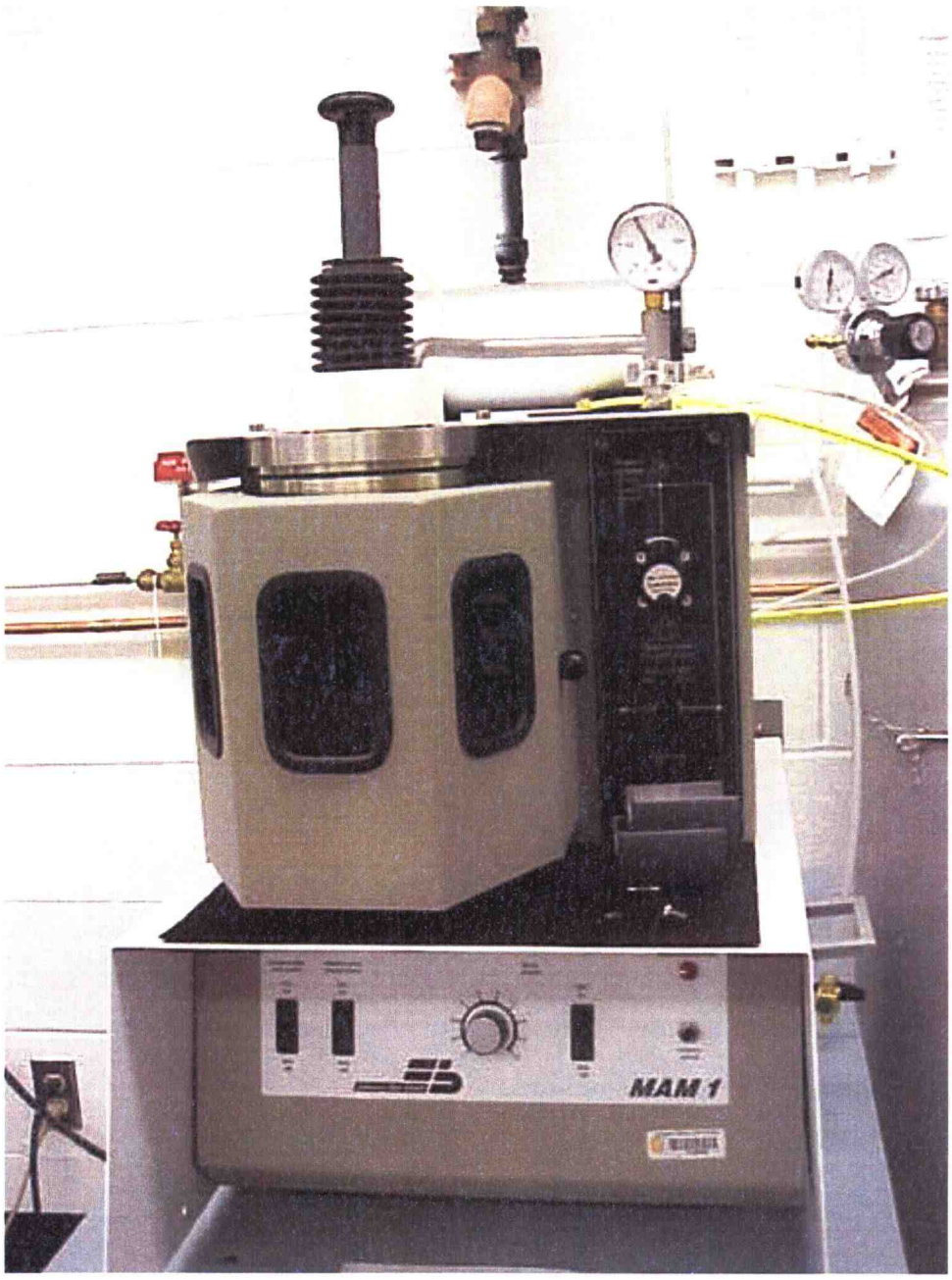

Figure 4 Laboratory Arc Melter.

3.1.2 Copper Boat System

The copper boat system works on the principle of induction heating where the heat is generated by producing eddy currents in an electrically conductive material. The master sample of $Zr_{58.5}Cu_{15.6}Ni_{12.8}Al_{10.3}Nb_{2.8}$ was prepared by inductively melting the elements in the water-cooled copper boat by applying RF-power through copper coil. Here, melting is carried out in protective argon atmosphere of 99.999% purity after evacuating it to high vacuum. The alloy is melted 3-4 times to ensure homogeneity. This technique allows good chemical homogeneity of the melt without any contamination.

In both methods titanium was used as an oxygen getter. The use of getter ensures prevention of constituent metal oxide formation. The glassy samples were then analyzed in the thermal analyzer.

3.2 Thermal Analysis

Thermal analysis involves a group of techniques to study thermal behavior of material and to measure physical sample properties when the sample is subjected to a predefined heating and cooling programme. It also traces the temperature dependent phenomenon such as decomposition, melting, crystallization, chemical reaction, glass transition and other phase transitions.

3.2.1 Differential Scanning Calorimetry (DSC)

The Differential Scanning Calorimetry (DSC) is a most widely used thermoanalytical technique. Perkin Elmer [49] Pyris DSC1 is a highly sensitive power compensated

differential scanning calorimeter that provides fundamentally sound measurement of heat flow as a function of time and temperature. Laboratory set-up for DSC is shown in Fig. 5.

3.2.1.1 WORKING PRINCIPLE

The sample and the reference have individual heaters and sensors to measure the power that is supplied in order to keep the sample and the reference at the same temperature during heating, cooling or isothermal cycles. Schematic of DSC is shown in Fig. 6. The temperature difference is maintained to nearly zero by varying the necessary power. This power is a measure of change in enthalpy or heat capacity of sample relative to reference. Also, temperature changes in the sample are recorded during exothermic or endothermic enthalpy transitions in terms of heat flow. It is more precise and accurate than DTA because it measures required power rather than the temperature difference between the sample and reference at identical temperatures. Furthermore, the height of the curve in DSC at any time t is a measure of heat evolving from sample per unit time instead of temperature difference ΔT between the specimen and the reference.[50]

Most of the experiments in DSC are performed either isothermally or with temperature changing at a constant rate. In isothermal experiments the DSC signal is plotted against time at each constant temperature. In dynamic experiments DSC signal is plotted against either time or temperature. Typical DSC scan obtained by continuously heating the bulk metallic glass specimen at a steady heating rate is shown in Fig. 7. Here, it depicts the phase transitions occurred during the first heating cycle. Initial small endothermal peak corresponds to glass transition T_g and provide the proof for initial glassy state of the specimen. Upon further heating crystallization occurs exothermally (heat release from the

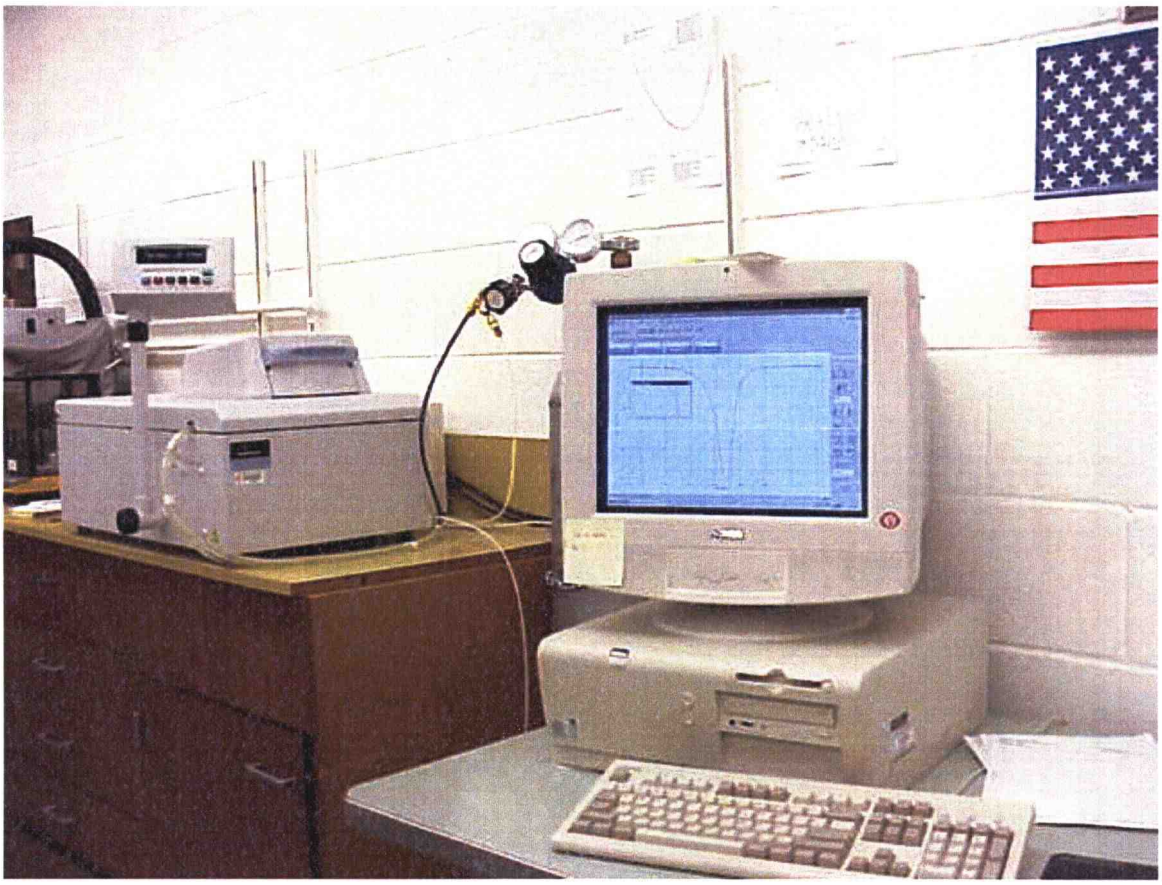

Figure 5 Laboratory set up for DSC.

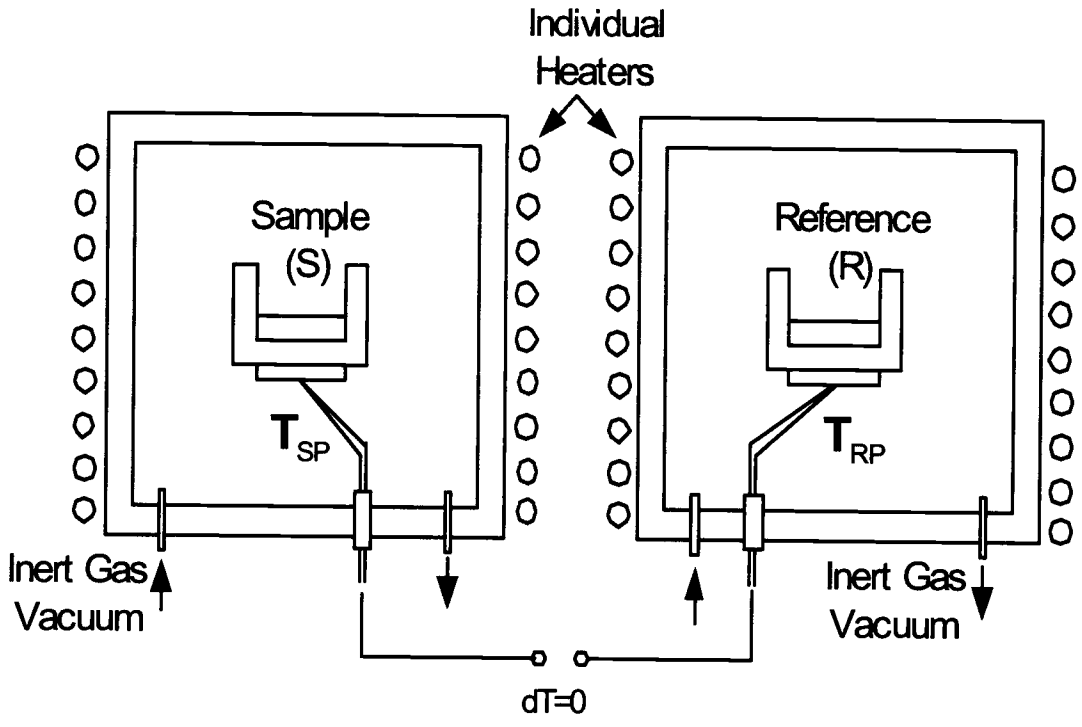

Figure 6 Schematic showing major components of DSC.
(Ref.: http://wwwswt.informatik.uni-rostock.de/englisch/projekte/Physik2000/ExperimentII/ta2web001.pdf)

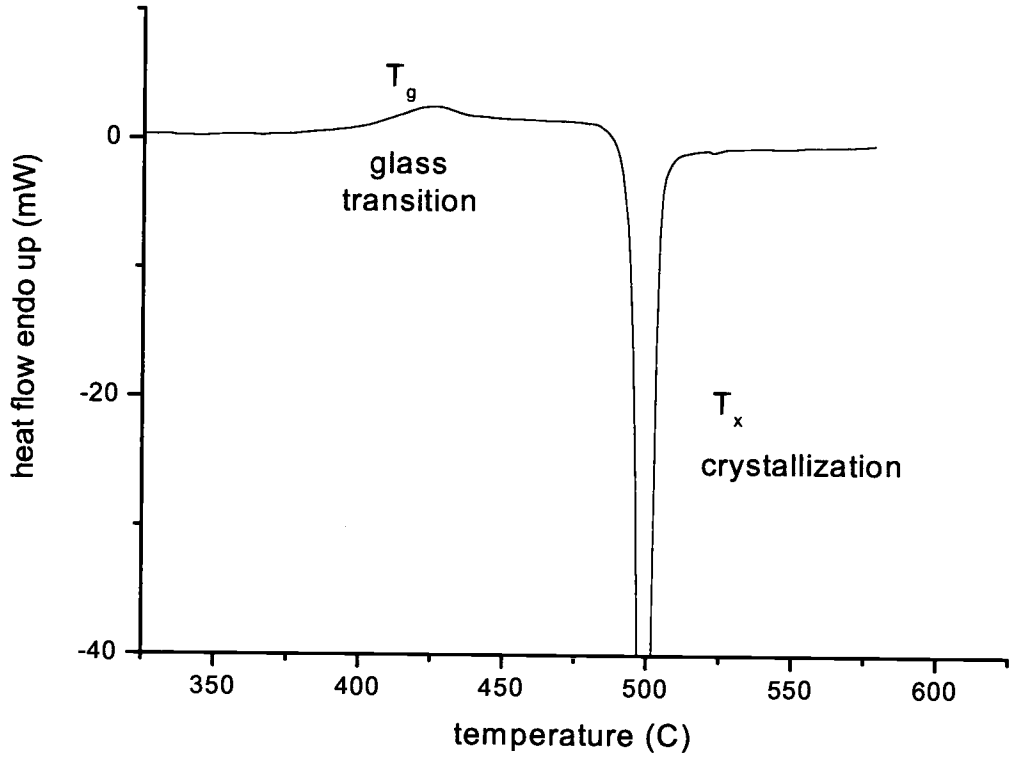

Figure 7 DSC thermogram of heat flow as a function of temperature. Initial endothermic peak corresponds to glass transition followed by exothermic crystallization peak.

specimen) which is shown by T_x followed by the endothermal (heat absorption) melting of the sample if the material has a melting point of less than 580 °C.

3.2.1.2 CALIBRATION

In order to get precise data it is necessary to calibrate the DSC accurately. The DSC is usually calibrated using substances with known melting points and calibration can be conveniently done in the required temperature range. Major calibration of the DSC involves temperature calibration and baseline calibration.

3.2.1.2.1 TEMPERATURE CALIBRATION

To maintain proper operating condition of the instrument, it is advisable to do temperature calibration every three to six months. Routine calibration comprises of Temperature Calibration and Heat Flow Calibration. The DSC machine is calibrated for different heating rates using highly pure reference materials whose physical properties are known. Selection of the reference material for optimal performance is crucial for the operating temperature range. In our calibration, we used very high purity Zinc and Indium (99.999%) having melting points of 419.47 °C and 156.60 °C respectively as reference material. The calibration procedure includes heating the sample at various heating rates through the melting temperature and carrying out enthalpy calculation and measuring onset temperature of melting for each heating rate and for each reference material. The measurement of onset temperature and enthalpy of fusion (ΔH_m) is required for temperature and heat flow calibration respectively. The enthalpy of fusion is calculated by integrating the area under the melting peak. The calibration was carried out using heating rate in the range of 0.033 K/s to 3.33 K/s. After taking required

measurements, melting temperature and enthalpy as a function of heating rate is plotted for Indium as shown in Fig. 8 and Fig. 9 respectively and finally instrument is programmed for corrected temperature shift. Similar procedure is followed for Zinc standard.

3.2.1.2.2 BASELINE CALIBRATION

Baseline calibration was carried out in order to optimize the baseline. It is necessary to select the temperature range over which the baseline needs to be optimized. In our case the useful temperature range was 200-600 °C. It involves baseline curvature correction and baseline slope adjustment. It is important to consider that during baseline calibration the sample holder and reference holder needs to be empty. In the baseline curvature correction, several baseline runs were carried out until most of the baseline curvature was gone by adjusting for peak height and end limits of curvature. Baseline slope adjustment was carried out until the baseline was straight and parallel with the X-axis.

3.2.1.3 SAMPLE PREPARATION FOR DSC

Most of the thermodynamic and kinetic calorimetric measurements of $Zr_{58.5}Cu_{15.6}Ni_{12.8}Al_{10.3}Nb_{2.8}$ are performed using Perkin Elmer Pyris DSC 1. Weight of the samples used for DSC analysis range from 90-170 mg. Samples are initially cleaned with ethyl alcohol in ultrasonic cleaner followed by acetone to remove any external sample contamination. The samples are allowed to dry and weighed precisely and finally placed in a high purity standard aluminum sample pan and covered securely with aluminum lid. Empty reference pan is of the same material as sample pan. Sample pan and empty

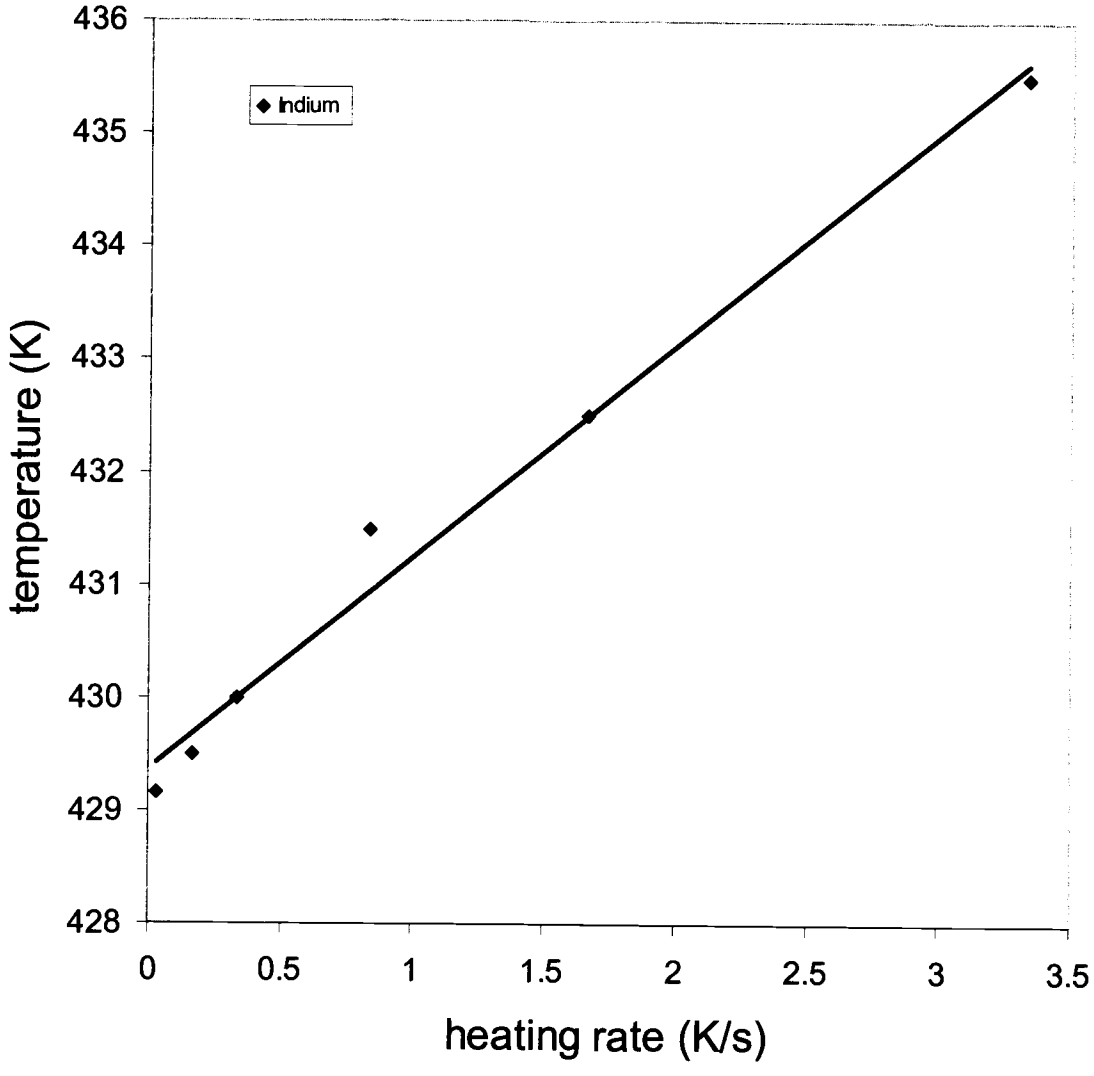

Figure 8 Calibration data of temperature vs. heating rate for Indium standard.

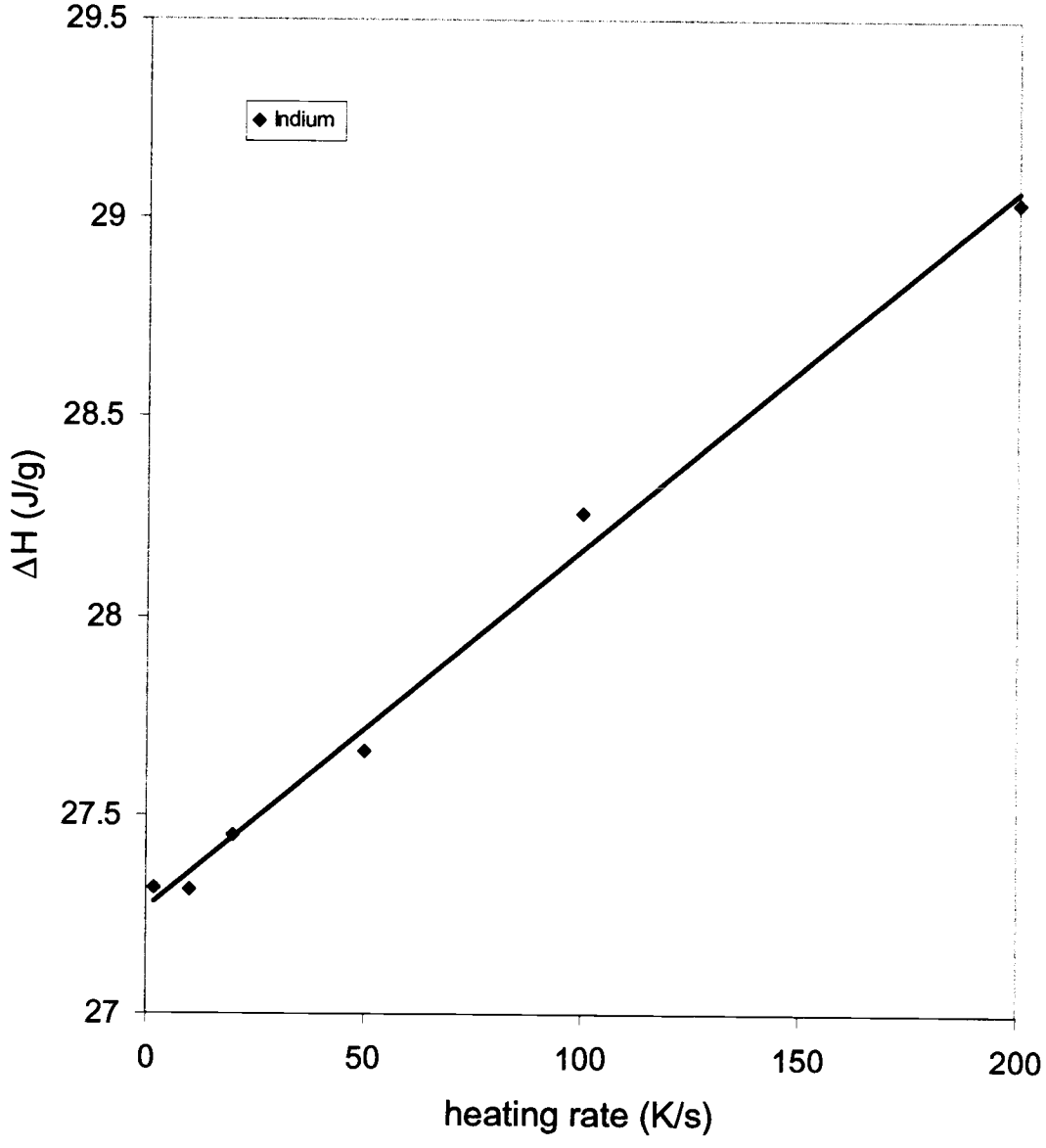

Figure 9 Calibration data of enthalpy vs. heating rate for Indium standard.

reference pan are then secured in a platinum sample holder and reference holder respectively. Both holders are then closed with vented platinum lid and covered with sample holder enclosure cover. During processing whole system is protected from any contamination by creating an argon (99.999%) ambience.

3.2.1.4 ACTUAL EXPERIMENTAL RUNS

In this study of $Zr_{58.5}Cu_{15.6}Ni_{12.8}Al_{10.3}Nb_{2.8}$ alloy isothermal measurements were done in the glassy region, calorimetric glass transition region as well as supercooled liquid region. Samples were first heated above the glass transition temperature into supercooled liquid state at a rate of 0.33 K/s and then cooled to room temperature at the same rate to give the samples the similar thermal history. This step is called Preannealing. The reason for heating all the samples to supercooled liquid region, which is observed between the melting point and the glass transition, is to establish its characteristic independence from previous history. Prior to and during each experiment the chamber was purged with 99.999% argon. In all isothermal experiments, samples were heated to the assigned temperature with a rate of 1 K/s. After relaxation and crystallization they were cooled back to room temperature. Fig. 10 shows a DSC scan in which four different regions are identified. The material is glassy below 667 K. The increase in the specific heat capacity (endothermic heat flow) between the temperatures of 667 K and 700 K indicate the region of calorimetric glass transition. Above 700 K material is in a supercooled liquid state and undergoes crystallization on further heating.

This work mainly focuses on the relaxation behavior of $Zr_{58.5}Cu_{15.6}Ni_{12.8}Al_{10.3}Nb_{2.8}$ in the glass transition temperature range. We developed an experimental method in which we

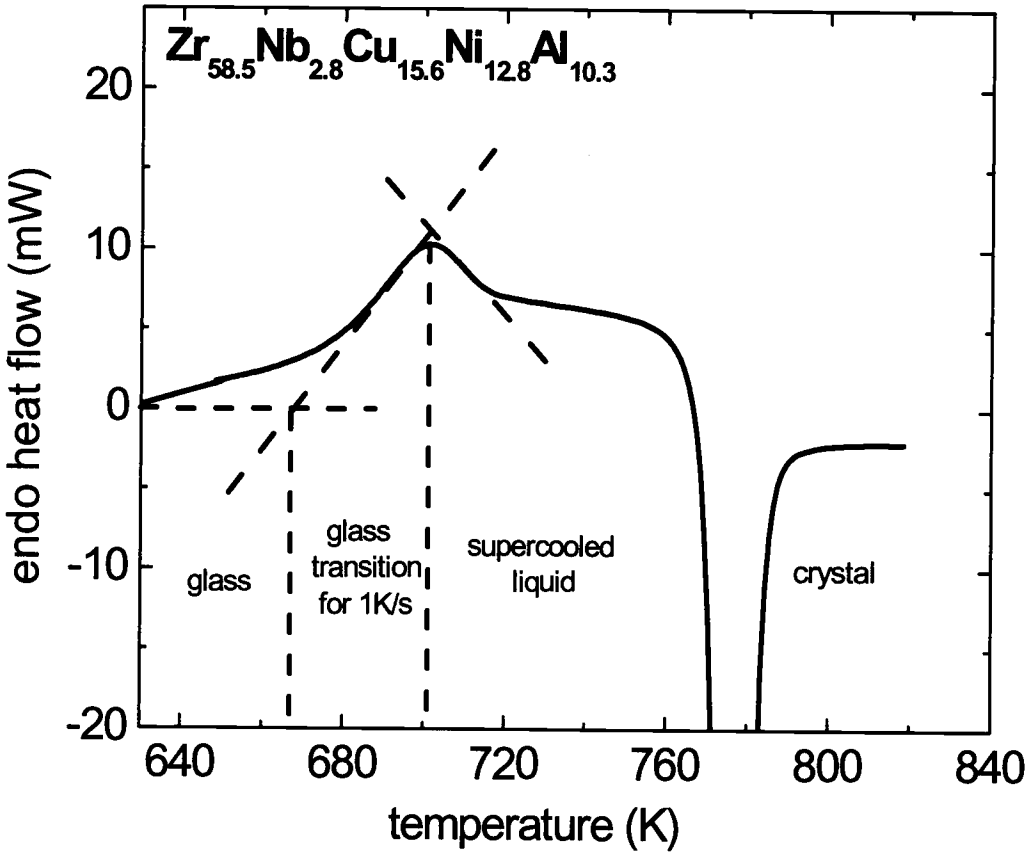

Figure 10 DSC scan of endothermic heat flow as a function of temperature in the glass transition region at a constant heating rate of 1 K/s.

can monitor enthalpy relaxation directly as a function of time. We thus get more information about relaxation than any previous studies, where enthalpy recovery was used. [51, 52] Fig. 11 depicts schematic diagram of heat flow (W/g-atom) versus time (sec) for isothermal measurements below the glass transition temperature. The solid line represents typical transition behavior when the glassy material undergoes enthalpy relaxation during isothermal anneal below the glass transition temperature. When the glassy sample is first heated at 1 K/s from room temperature (323 K) to the assigned isothermal temperature, heat flux reaches to point A. As soon as the material reaches to isothermal temperature, there is a sudden drop in the heat flux signal to B and it starts releasing heat until it reaches equilibrium supercooled liquid state C. This transition from B to C where the material transforms from glassy state to the supercooled liquid state is termed enthalpy relaxation, which is shown by downward lip region of the curve. On continued heating to isothermal temperatures for long time, it undergoes crystallization that is revealed by the exothermic heat release peak D. A base line run was carried out immediately after sample run by providing similar isothermal conditions. The dashed line on top of the solid one represents the baseline.

3.2.1.5 SPECIFIC HEAT CAPACITY MEASUREMENT

The power compensated DSC measures specific heat capacity of $Zr_{58.5}Cu_{15.6}Ni_{12.8}Al_{10.3}Nb_{2.8}$ sample at constant pressure. Absolute heat capacity measurements were carried out for glass samples as well as crystalline samples. Sapphire was used as a standard for this calculation. Four experimental runs were performed using exactly same thermal conditions. First run was carried out using sapphire (highly pure

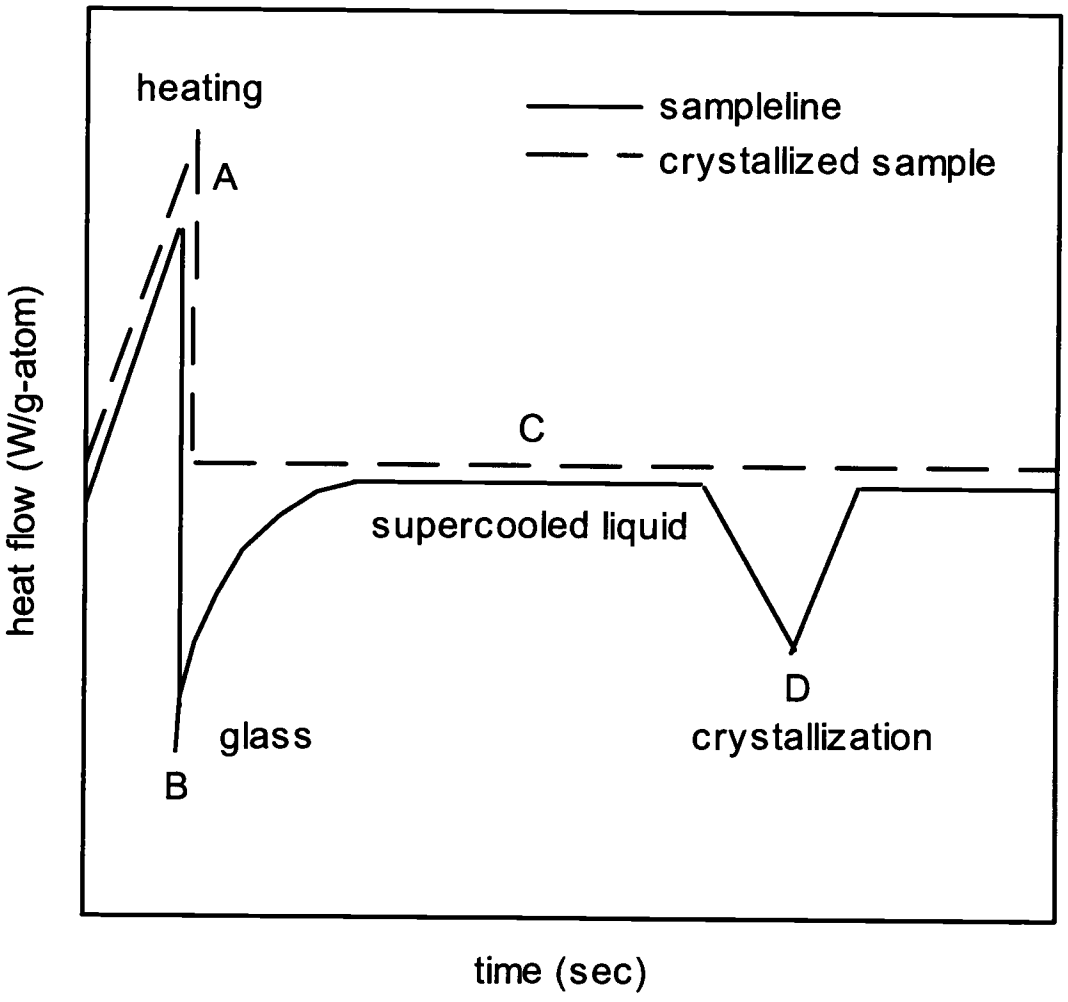

Figure 11 Schematic diagram of heat flow versus time depicts how the amorphous material relaxes from glassy state into equilibrium supercooled liquid state when isothermally annealed below the glass transition temperature. The sample undergoes crystallization if held long enough in equilibrium supercooled liquid state. Solid line is indicative of sample run and dotted line represents baseline run of the crystallized sample.

Al_2O_3) standard and second run for constructing baseline using two empty reference aluminum pans. Third and fourth run were performed using glassy and crystalline sample respectively. Baseline run was subtracted from Sapphire run, glassy run and crystalline run to get absolute value of specific heat. The method for experimental runs comprises of heating the sample at a constant heating rate of 0.33 K/s up to certain temperature and holding isothermally for 120 sec at that temperature. This resulted in a step of the heat flux dQ/dt [53,54]

$$\frac{dQ}{dt} = \left(\frac{\partial Q}{\partial t}\right)_{\dot{T}\neq 0} - \left(\frac{\partial Q}{\partial t}\right)_{\dot{T}=0} = C \cdot \frac{dT}{dt} \tag{16}$$

here, $\left(\frac{\partial Q}{\partial t}\right)_{\dot{T}\neq 0}$ is the necessary power to heat and hold the sample and the pan at a certain temperature and $\left(\frac{\partial Q}{\partial t}\right)_{\dot{T}=0}$ is the required power to keep the temperature constant and C is the heat capacity of sample and pan.

Following formula was used to calculate the specific heat capacity of the sample

$$C_p(T)_{sample} = \frac{\dot{Q}_{sample} - \dot{Q}_{pan}}{\dot{Q}_{sapphire} - \dot{Q}_{pan}} \cdot \frac{m_{sapphire} \cdot \mu_{sample}}{m_{sample} \cdot \mu_{sapphire}} \cdot C_p(T)_{sapphire} \tag{17}$$

where, m is the mass, μ the molecular weight and $C_p(T)_{sapphire}$ the standard specific heat capacity of sapphire obtained from literature. This procedure was carried out every 20K.

3.2.2 Differential Thermal Analysis (DTA)

Differential Thermal Analysis (DTA) measurements were carried out near the liquidus temperature due to the inability of the DSC to go to higher temperatures. DTA is used to

measure thermodynamic properties when subjected to controlled heating and cooling at various temperatures. The main components of the machine include a metallic or ceramic blocks to ensure uniform heat distribution, sample and reference crucibles and thermocouples, inert gas system and PC or plotter for data acquisition.

3.2.2.1 WORKING PRINCIPLE

DTA as the name suggest measures the temperature difference between sample and the reference (a thermally inert material) when heated or cooled under identical conditions. The temperature difference is then plotted against time or temperature. This is the most useful method for determining precise reaction temperature of exothermic or endothermic events, phase change as well as enthalpy change at high temperatures. A schematic sketch of DTA is shown in Fig. 12. Heating or cooling is carried out in an argon atmosphere. The shape of the DTA peak depends on sample weight and heating rate employed.

3.2.2.2 CALIBRATION

Similar to the DSC, the DTA machine is subjected to both temperature calibration and baseline calibration. Baseline calibration was performed using empty sample and reference pan. For the temperature calibration four high purity metals namely Zn, Al, Ag and Cu were used. The true melting point of the standards was measured at the onset of the melting peak. The melting peak area is determined for correcting enthalpy of fusion. Fig. 13 shows the calibration curve that was used to correct for the enthalpy of fusion. Experimental runs were carried out from room temperature to well above their melting

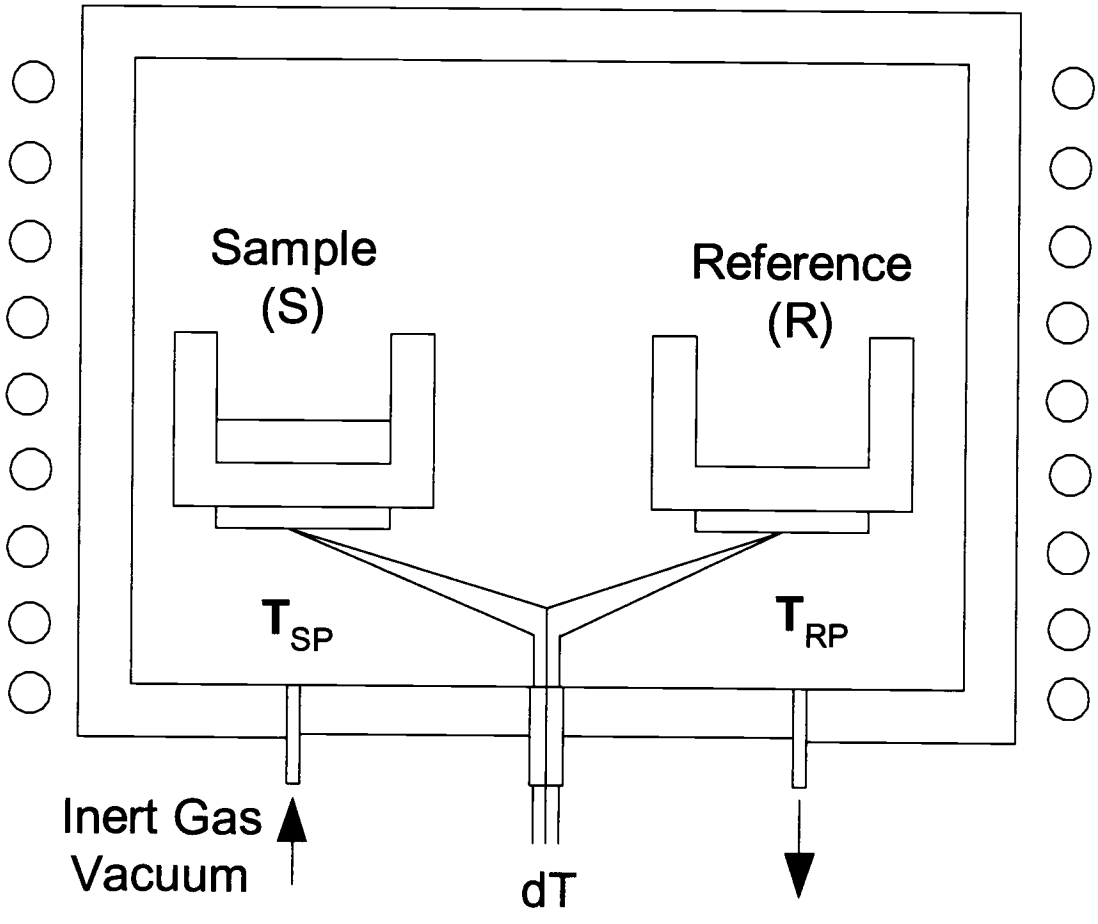

Figure 12 Schematic of Differential Thermal Analyzer (DTA).
(Ref.: http://wwwswt.informatik.uni-rostock.de/englisch/projekte/Physik2000/ExperimentII/ta2web001.pdf)

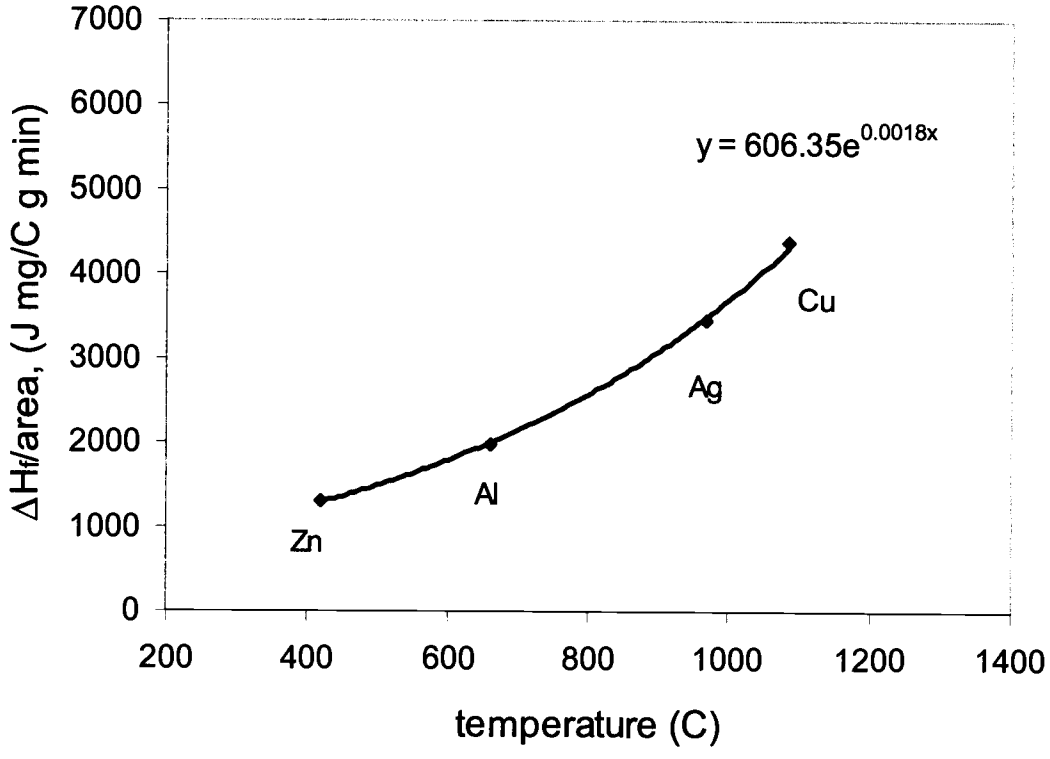

Figure 13 Enthalpy calibration curve fitted by measuring peak area of highly pure metals with increasingly high melting point.

points at constant heating rate of 0.33 K/s. Their melting temperatures and melting peak area was measured. This curve is generated to correct for the apparent smaller ΔH_f with increase in temperature. For each metal ΔH_f was calculated by integrating the melting peak area and onset of melting peak was recorded. ΔH_f value for each metal is then plotted against their respective melting temperature followed by fitting with the exponential function.

4 RESULTS

4.1 Thermodynamics

The thermodynamics of $Zr_{58.5}Cu_{15.6}Ni_{12.8}Al_{10.3}Nb_{2.8}$ bulk metallic glass forming alloy is studied by experimentally measuring the specific heat capacity data using the DSC at constant heating rate and deriving various thermodynamic functions from it. In addition, experiments were carried out on $Zr_{58.5}Cu_{15.6}Ni_{12.8}Al_{10.3}Nb_{2.8}$ at various heating rates from room temperature to melting temperature using DSC and DTA.

4.1.1 Experimental Details

4.1.1.1 ACTUAL REPRESENTATIVE DTA SCAN FOR $Zr_{58.5}Cu_{15.6}Ni_{12.8}Al_{10.3}Nb_{2.8}$

In most of the thermodynamic experiments of $Zr_{58.5}Cu_{15.6}Ni_{12.8}Al_{10.3}Nb_{2.8}$, the sample was heated from room temperature to the crystallization temperature in DSC with different heating rates but in order to know its thermal behavior at higher temperatures some of the experiments were also carried out with the DTA up to the melting point. Fig. 14 shows a typical DTA thermogram at a heating rate of 0.33 K/s. The initial endothermic peak of glass transition at 668 K represents the softening of the material. It occurs over a range of temperatures. On continued heating to higher temperatures the glass transition is followed by two exothermic peaks of crystallization, where the supercooled liquid transforms into the crystalline mixture. The onsets of primary and

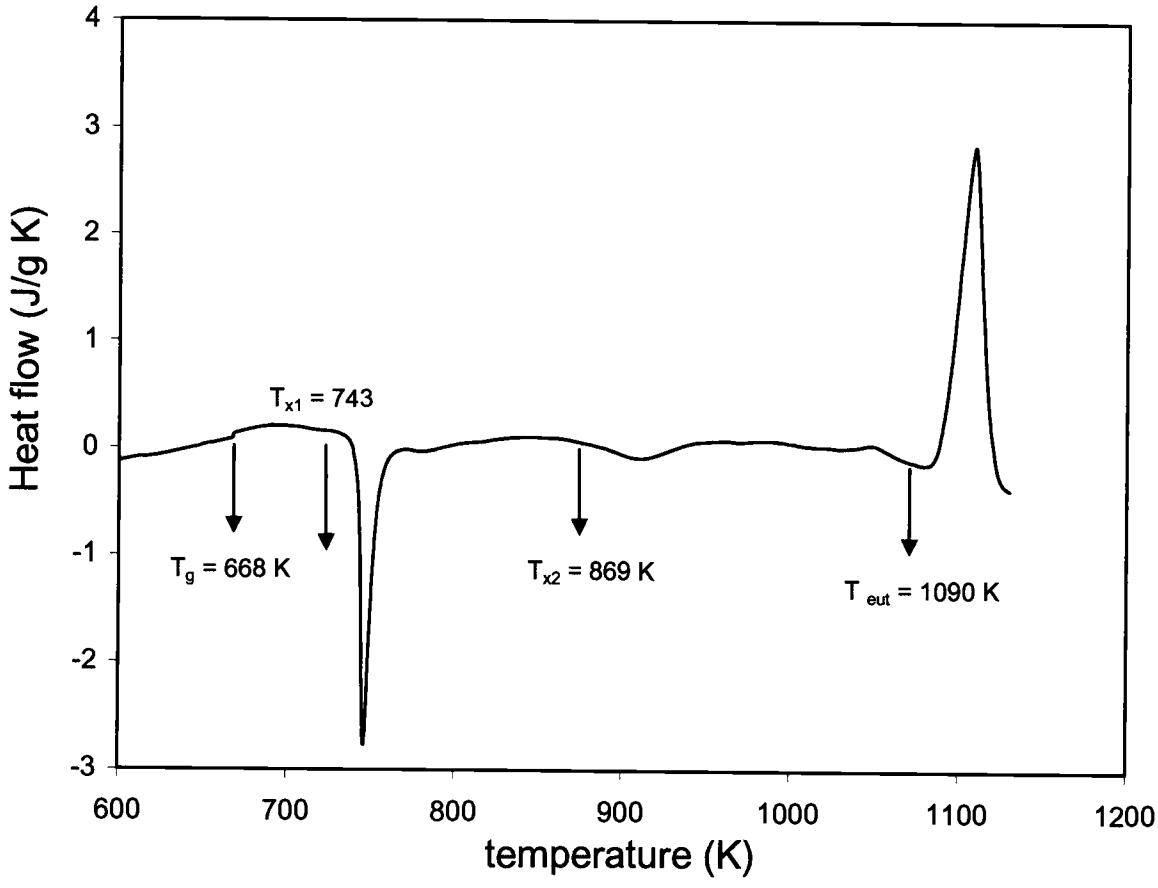

Figure 14 DTA thermogram as a function of temperature for bulk metallic glass $Zr_{58.5}Cu_{15.6}Ni_{12.8}Al_{10.3}Nb_{2.8}$ at a heating rate of 0.33 K/s. T_g represents the onset of glass transition along with two-crystallization events T_{x1} and T_{x2}. T_{eut} represents the eutectic temperature.

secondary crystallization peaks are observed at 743 K and 869 K respectively. The primary crystallization peak is sharp and narrow while the secondary crystallization peak is wider and smaller. The presence of a stepwise transformation during crystallization might be indicative of phase separation as this is a commonly observed phenomenon in other glass forming alloys.[55] The eutectic temperature (T_{eut}) at which the alloy starts to melt is observed at 1090 K followed by complete melting at the liquidus temperature (T_{liq}) of 1124 K.

4.1.1.2 SPECIFIC HEAT

As described in section 3.2.1.5 three experimental runs were performed on glass and crystalline samples of $Zr_{58.5}Cu_{15.6}Ni_{12.8}Al_{10.3}Nb_{2.8}$ with reference to sapphire using the DSC to determine the specific heat capacity of supercooled liquid, glassy alloy and crystalline solid. Fig. 15 shows the specific heat capacity of $Zr_{58.5}Cu_{15.6}Ni_{12.8}Al_{10.3}Nb_{2.8}$ as a function of temperature for supercooled, glassy and crystalline state. Here, the specific heat capacity difference between supercooled liquid and crystal represents the difference between heat of fusion and heat of crystallization.[53] As depicted in Fig. 15 T_f represents the temperature of $Zr_{58.5}Cu_{15.6}Ni_{12.8}Al_{10.3}Nb_{2.8}$ at which the free energy of liquid and crystal are equal, T_g the onset of the glass transition temperature and T_k the Kauzmann temperature. As T_f for this alloy is not known exactly, the peak temperature of the melting peak is taken as T_f. The Kauzmann temperature [37] is also known as isentropic temperature and it is obtained here at the point where the entropy difference between

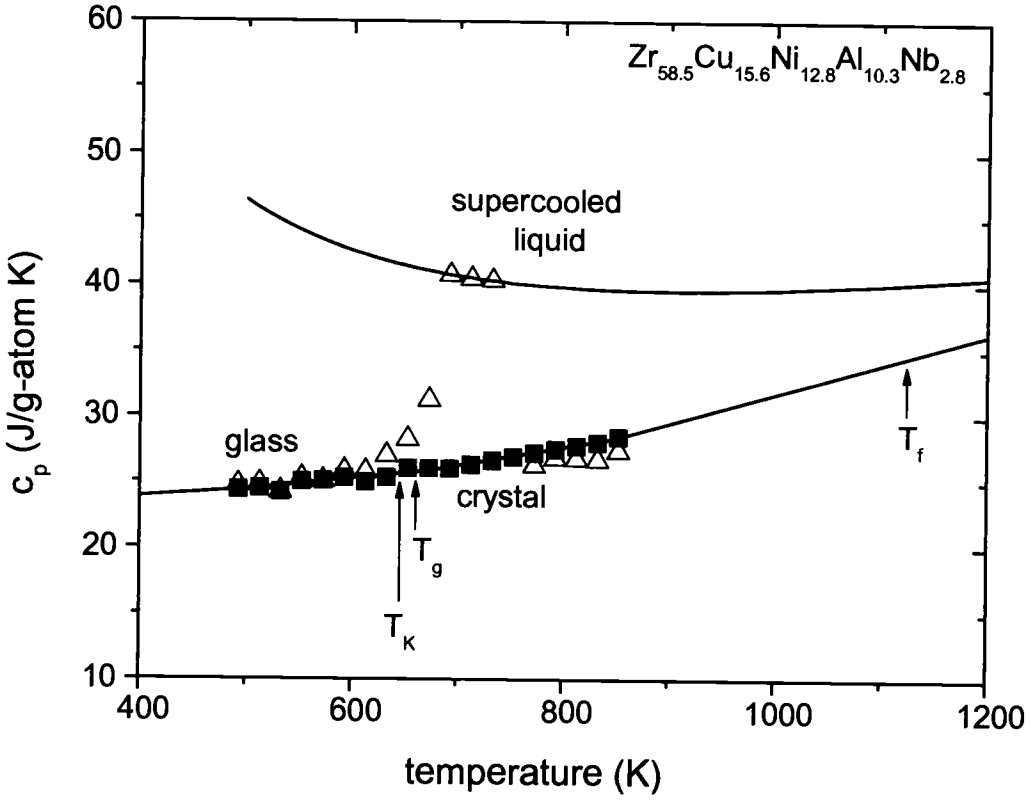

Figure 15 Quantified specific heat capacity of glassy state, supercooled liquid and crystalline solid as a function of temperature. The solid line represents the fitting to the respective data. (Δ) represents the experimental data points obtained during amorphous sample run and (■) during crystalline sample run. T_k, T_g and T_f stand for Kauzmann temperature, glass transition temperature and melting temperature respectively.

supercooled liquid and that of crystal vanishes. As described by Kubaschewski et. al.,[56] far above Debye temperature the specific heat capacity's dependence on temperature in the supercooled liquid region is expressed by

$$c_p^{\,l}(T) = 3R + a \cdot T + b \cdot T^{-2} \tag{19}$$

and the specific heat capacity of crystal is described by the equation

$$c_p^{\,x}(T) = 3R + c \cdot T + d \cdot T^{2} \tag{20}$$

in which, R = 8.3145 J/g atom K is the gas constant. The value of constants a and b are obtained by fitting the data in the supercooled liquid region and that of c and d by fitting crystalline data. The data of the supercooled liquid fitted using Equation 19 and for crystalline solid using Equation 20 is presented by the solid line. Value of a, b, c and d are found to be 0.0107, 4.01E6, -0.0081 and 1E-5 respectively in appropriate units. The rising of c_p with falling temperature in the supercooled liquid region is terminated near the glass transition temperature T_g. In contrast, specific heat value of glassy solid is close to crystalline at low temperatures and increases with increase in temperature. The difference in the specific heat between supercooled liquid and crystalline solid, which is 15.86 J/g-atom K near the glass transition temperature gradually reduces to less than half the value at fusion temperature and becomes minimal if extrapolated to higher temperatures.

4.1.2 Thermodynamic Functions

The thermodynamic functions can be estimated by calculating the specific heat capacity difference between the liquid and crystalline state as a function of temperature. Fig. 15 is used as a reference for calculation in sections 4.1.2.1, 4.1.2.2, 4.1.2.3 and 4.1.2.4.

4.1.2.1 CHANGE OF ENTHALPY DIFFERENCE WITH TEMPERATURE

By setting the enthalpy of the crystal as zero, it is possible to calculate the enthalpy difference between the supercooled liquid and crystal from eutectic point down to the glass transition temperature. The enthalpy difference at a particular temperature is given by

$$\Delta H^{l-x}(T) = \Delta H_f - \int_{T}^{T_f} \Delta c_p{}^{l-x}(T')dT' \tag{21}$$

where, ΔH_f is the heat of fusion and is obtained by calculating area under the melting peak. The last term in above Equation 21 can be evaluated at desired temperature from specific heat capacity calculation of $c_p{}^{l}(T)$ and $c_p{}^{x}(T)$ as shown in the previous section 4.1.1.2. Enthalpy change as a function of temperature is shown in Fig. 16. Here, T_f, T_g and T_k are the melting temperature, glass transition temperature and Kauzmann temperature respectively. The enthalpy difference between the supercooled liquid and crystal decreases towards the glass transition temperature. The enthalpy difference remains nearly constant below the glass transition temperature T_g. The residual enthalpy that is frozen-in during undercooling to glass transition temperature as shown in Fig. 16, can be relaxed to energetically favorable state by isothermal annealing. The amount of frozen-in enthalpy increases with increase in cooling rate.

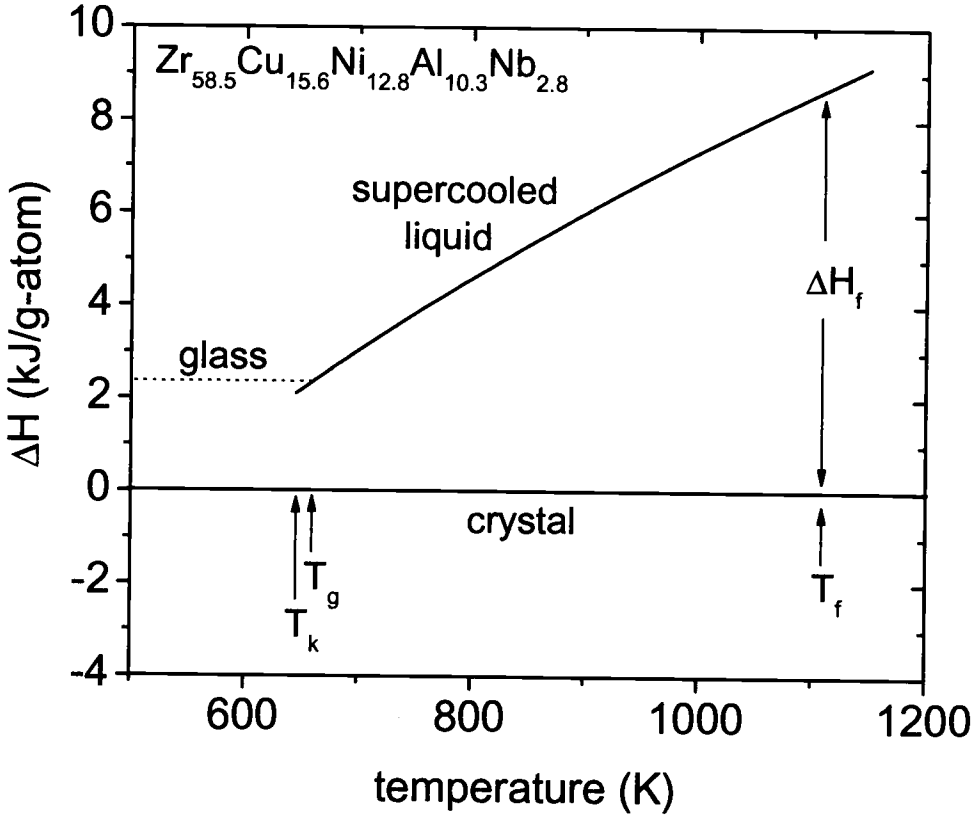

Figure 16 Enthalpy difference of supercooled liquid with respect to crystal as a function of temperature. T_k, T_g and T_f are Kauzmann temperature, glass transition temperature, and melting temperature respectively. ΔH_f designates the enthalpy of fusion.

4.1.2.2 CHANGE OF ENTROPY DIFFERENCE WITH TEMPERATURE

The entropy of the undercooled liquid with respect to the crystalline state is calculated by considering entropy of fusion as well as dependence of the specific heat on the temperature as indicated in Equation 22. Here, the entropy of the crystal is set as zero.

$$\Delta S^{l-x}(T) = \Delta S_f - \int_T^{T_f} \frac{\Delta c_p{}^{l-x}(T')}{T'} dT' \tag{22}$$

Entropy of fusion ΔS_f is calculated using,

$$\Delta S_f = \frac{\Delta \mathrm{H}_f}{T_f} \tag{23}$$

As shown in Fig. 17 the entropy of the liquid decreases with decreasing temperature and becomes equal to that of the crystal at Kauzmann temperature T_k (or isentropic temperature). It follows the same trend as that of enthalpy difference. The entropy can be extrapolated further down to VFT temperature T_0 but in doing that entropy of the liquid becomes smaller than that of the crystal. In order to avoid this so called Kauzmann paradox one must observe a drop in specific heat c_p at a temperature above the Kauzmann temperature in order for entropy of the glass to remain positive.[20] Also, it is a lower bound for estimating how far the liquid can be supercooled before the glass transition intervenes.[52]

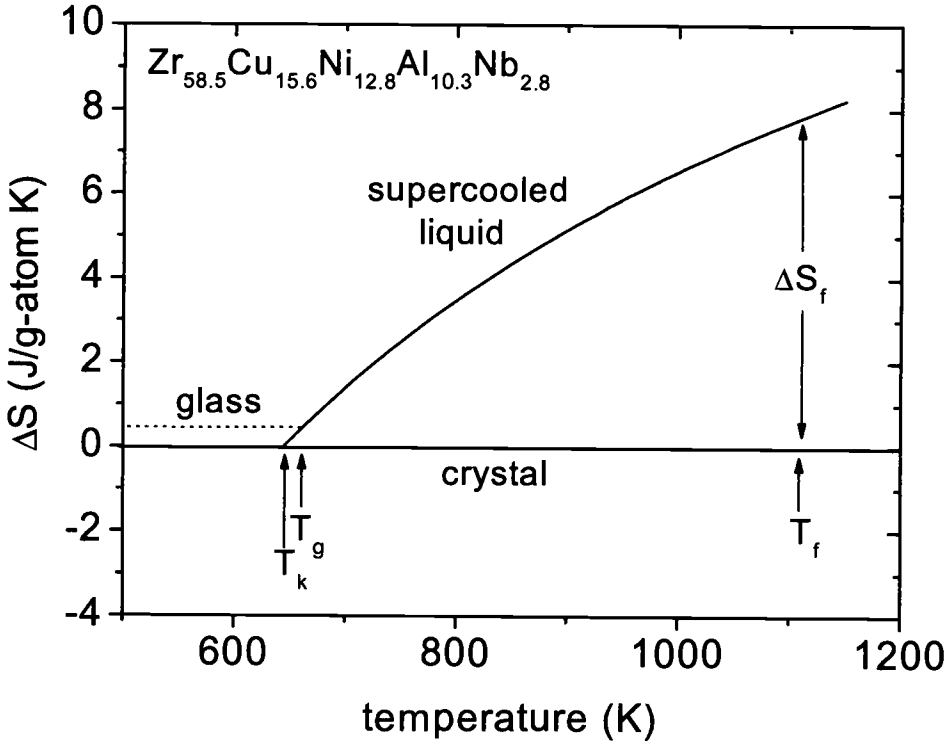

Figure 17 Change in entropy of supercooled liquid with respect to the crystal as function of temperature. T_k, T_g and T_f are Kauzmann temperature, glass transition temperature, and melting temperature respectively. ΔS_f indicates the entropy of fusion.

4.1.2.3. CHANGE OF GIBBS FREE ENERGY DIFFERENCE WITH TEMPERATURE

The Gibbs free energy of the supercooled liquid with respect to the crystal as a function of temperature $\Delta G^{l-x}(T)$ can be estimated by considering the enthalpy and entropy contribution from the above-mentioned calculations as indicated in the following equation

$$\Delta G^{l-x}(T) = \Delta H^{l-x}(T) - T \cdot \Delta S^{l-x}(T) \tag{24}$$

From Fig.18 it is evident that the Gibbs free energy change ΔG diminishes with increasing temperature and the energy difference between liquid and solid become equal at the melting temperature T_f. The smaller slope of the Gibbs free energy curve just below the melting point for this alloy due to its relatively small entropy of fusion is indicative of a small driving force for crystallization and thus high glass forming ability. Co-relating this to specific heat capacity curve of Fig.15, the increasing specific heat capacity difference between the melt and the crystal on larger undercooling reflects the stabilization of undercooled melt relative to the crystalline mixture.

4.2 Kinetics

Isothermal measurements or small heating rates are used to study the kinetic property of the material close to the glass transition. In this research, the kinetic studies of $Zr_{58.5}Cu_{15.6}Ni_{12.8}Al_{10.3}Nb_{2.8}$ alloy involves heating rate experiments as well as isothermal experiments to study the kinetics of relaxation and that of the crystallization using DSC

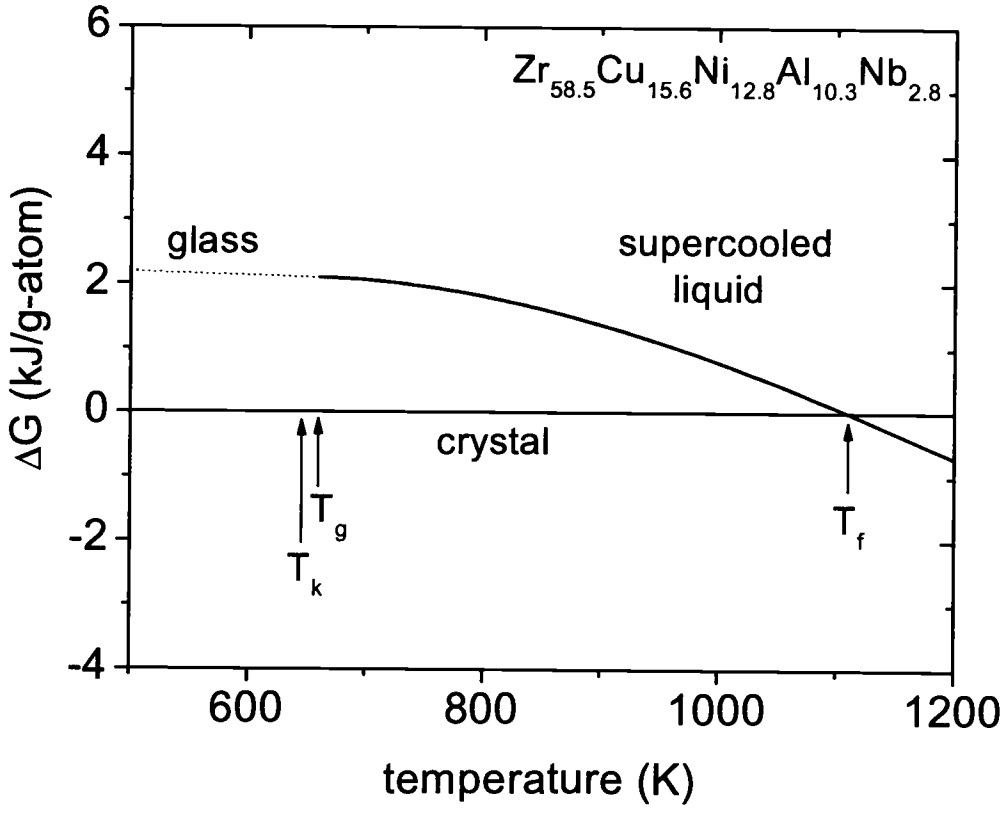

Figure 18 Gibbs free energy difference between supercooled liquid and crystal as a function of temperature for $Zr_{58.5}Cu_{15.6}Ni_{12.8}Al_{10.3}Nb_{2.8}$. T_k, T_g and T_f are Kauzmann temperature, glass transition temperature, and melting temperature respectively.

and DTA. Isothermal relaxation experiments were carried out below the onset glass transition temperature and crystallization runs were performed in the glass transition and supercooled liquid region.

4.2.1 Heating Rate Kinetics

4.2.1.1 EFFECT ON GLASS TRANSITION AND CRYSTALLIZATION TEMPERATURE

The location of glass transition and crystallization temperature depends on the heating or cooling rate. In our experiments the glass transition and crystallization shifts were studied with different heating rates in the range of 8.33×10^{-3} and 3.33 K/s. The glass transition and crystallization are shifted to higher temperatures with increase in heating rate as shown in Fig. 19. As the transformation occurs over a range of temperature in both cases, three characteristic points named onset, the point of steepest accent or peak and end temperatures were measured for each transition and for different heating rates as shown in Fig. 20. The onset temperature is defined as the intersection of the steepest slope of the low-temperature part of the peak and the baseline. In addition, the width of the supercooled liquid region also increases with heating rate. As shown here, supercooled liquid region begins at the end of glass transition transformation and ends at the point where crystallization initiates.

4.2.1.2 FRAGILITY PLOT AND VFT EXPRESSION

The heating rate data are best fitted with the Vogel-Fulcher-Tammann (VFT) type relation, which is given by,[57]

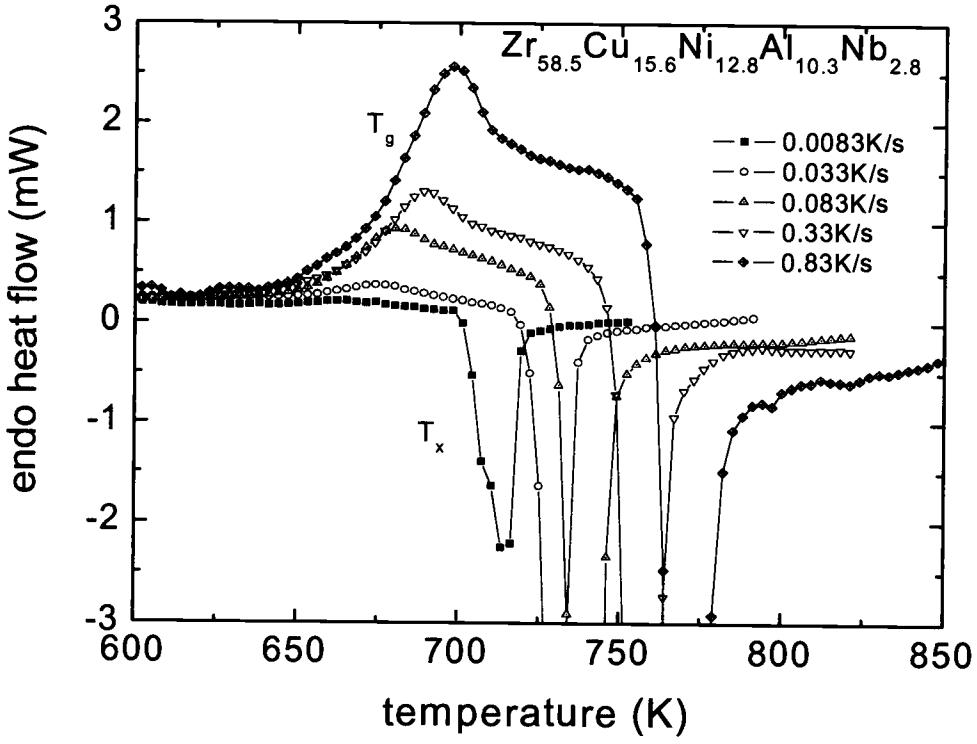

Figure 19 DSC scans of shift in glass transition and crystallization with temperature as a function of heating rate. Initial endothermic peak designates glass transition (T_g) phenomenon followed by exothermic event of crystallization (T_x).

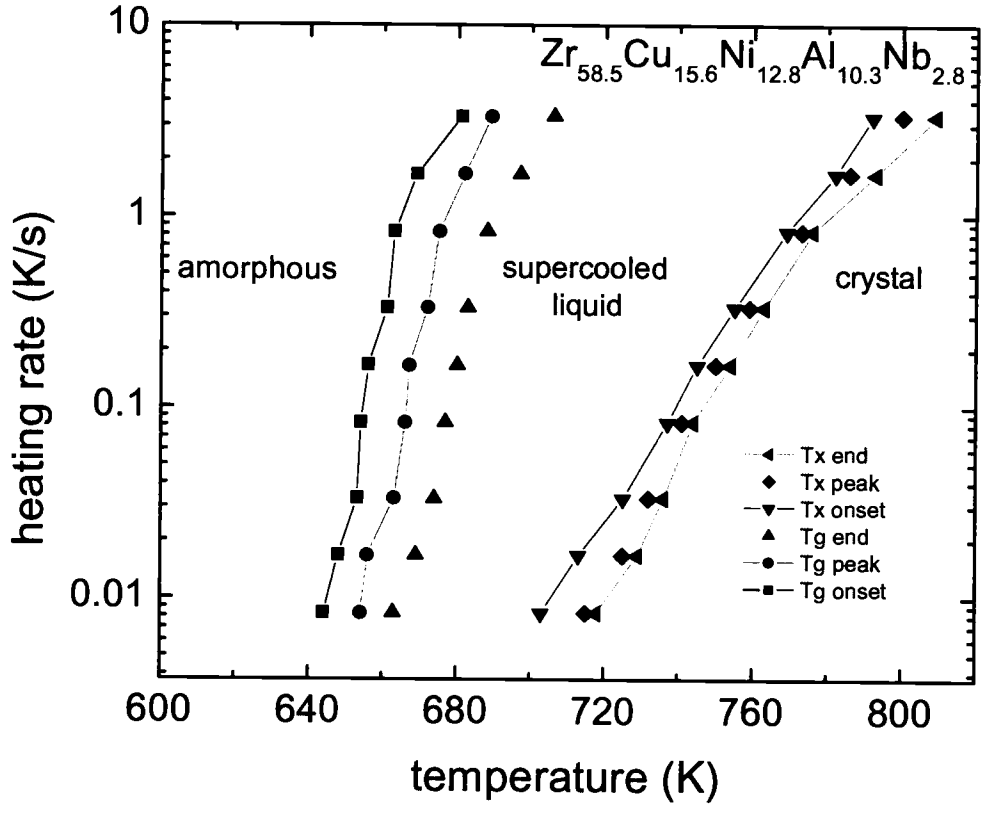

Figure 20 Variation of onset, peak and end temperature of glass transition Tg and crystallization T_x with heating rate for $Zr_{58.5}Cu_{15.6}Ni_{12.8}Al_{10.3}Nb_{2.8}$

$$\tau = \tau_0 \cdot \exp\left(\frac{D^* \cdot T_0}{T - T_0}\right) \tag{25}$$

here, τ_0 is a pre-exponential factor, D^* is the fragility parameter and T_0 is the VFT-temperature. Value of τ_0 is fixed to $4*10^{-14}$ throughout the fitting. Plot of relaxation time τ as a function of glass transition temperature is shown in Fig. 21. Here the relaxation time of calorimetric glass transition is approximated by normalizing the width of the glass transition region ΔT_g with heating rate R (K/s),

$$\tau = \frac{T_g^{onset} - T_g^{end}}{R} = \frac{\Delta T_g}{R} \tag{26}$$

By fitting the data with the VFT-equation in fragility plot value of D^* is found to be 19.7 and T_0 436.8 K.

4.2.2 Relaxation Kinetics

As $Zr_{58.5}Cu_{15.6}Ni_{12.8}Al_{10.3}Nb_{2.8}$ has better resistance to crystallization in its supercooled and glass transition region, [8] it is possible to study relaxation from the glassy state into the supercooled liquid state. Measurements of isothermal enthalpy relaxation experiments of $Zr_{58.5}Cu_{15.6}Ni_{12.8}Al_{10.3}Nb_{2.8}$ carried out in the glass transition temperature range shows that sample gets isothermally relaxed from glassy state into the supercooled liquid state. In our experiments it is possible to carry out isothermal annealing only 30-40 K below the glass transition temperature. Far below the glass transition temperature noise to signal ratio in DSC increases to the extent that it is difficult to accurately measure the heat flux

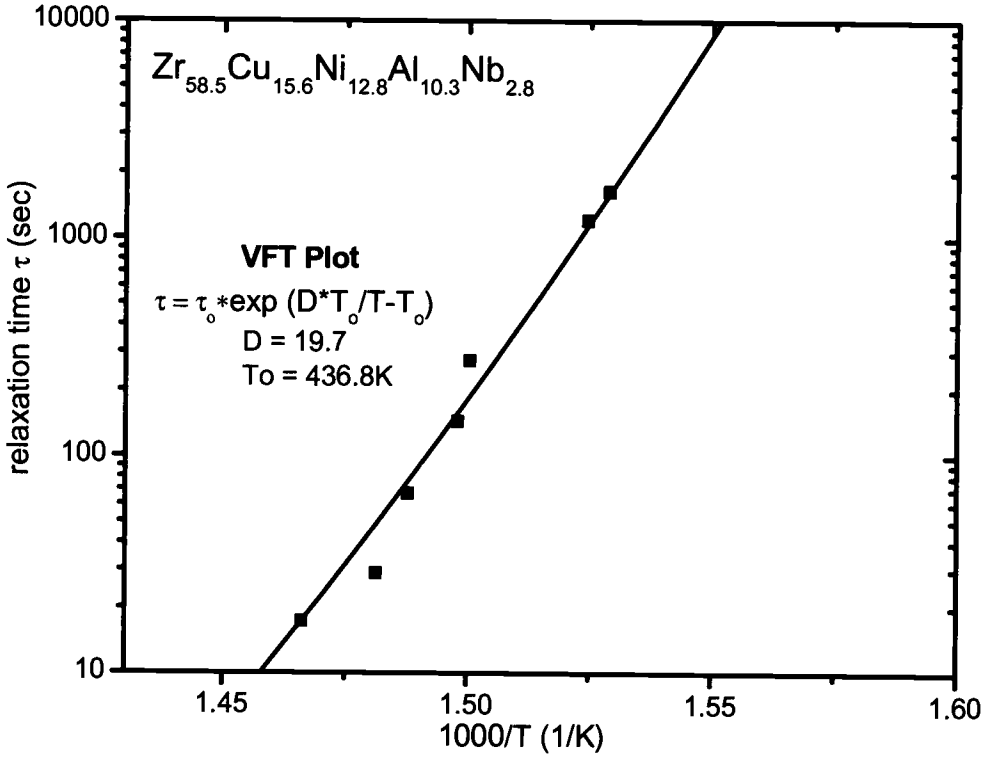

Figure 21 Fragility plot of the relaxation time at the glass transition as a function of inverse temperature. Fitting data with the VFT relation yields fragility parameter D of 19.7 and VFT temperature T_0 of 436.8 K.

towards the end of transformation and hence it becomes difficult to fit the curve with a stretched exponential function.

The sample is allowed to undergo relaxation by isothermal annealing in order to measure equilibrium enthalpy near the glass transition temperature. The Y-ordinate on the DSC scan represents the heat flux Q^0 (J/sec). It is given by

$$Q^0 = m \cdot c_p \cdot \dot{T} \tag{27}$$

where, m = sample weight (mg), c_p = specific heat of the sample (J/g-atom K) and $\dot{T}$ = the heating rate (K/s).

Heat flow Q is calculated by integrating heat flux over a period of time from the glassy state to the supercooled liquid state where the change in heat flux becomes zero as shown in Equation (28). The time at which relaxation starts from the glassy state is designated by t_{glass} and at times where material reaches the supercooled liquid state, is designated by $t_{supercooled}$

$$Q^0 = \int_{t_{glass}}^{t_{supercooled}} \frac{dQ}{dt} dt = Q \tag{28}$$

where, Q^o = Heat flow rate or heat flux (J/s), Q = Heat flow (J).

Being the extensive property, enthalpy is directly proportional to the quantity of the material in the system. So, to calculate the enthalpy, the heat flow Q is normalized by the sample weight and multiplied by the molecular weight of $Zr_{58.5}Cu_{15.6}Ni_{12.8}Al_{10.3}Nb_{2.8}$ to get the enthalpy in J/g-atom. It is found that the relaxation process obeys stretched exponential function and it does not proceed exponentially with time.[47] Here the enthalpy

relaxation is fitted with stretched exponential function which is very similar to the function that is used for the viscosity relaxation. Equation (15)

$$H(t) = H_g - \Delta H_{total} \cdot (1 - e^{-(t/\tau)^{\beta}}) \tag{29}$$

where, τ = average relaxation time, β = a stretching exponent, t = time, $H(t)$ = enthalpy as a function of time, H_g = enthalpy of the glass before relaxation, ΔH_{total} = total enthalpy change during relaxation from glassy state into equilibrium supercooled liquid state. After calculating the enthalpy change for all the isothermal runs carried out below the glass transition region, it is plotted as a function of time and two useful fitting parameters named relaxation time (τ) and stretching exponent beta (β) that help in predicting the glass forming ability of $Zr_{58.5}Cu_{15.6}Ni_{12.8}Al_{10.3}Nb_{2.8}$ are obtained by fitting with the stretched exponential function Equation (29). Fig. 22 shows the fitted curve of normalized enthalpy change $\Delta H/\Delta H_{(total)}$ versus time at a temperature of 661 K. The fitting equation used here is given by

$$\Delta H / \Delta H_{(total)} = 1 - e^{-(t/\tau)^{\beta}} \tag{30}$$

This equation is similar to Equation (29) but for simplicity ΔH is normalized with respect to the total enthalpy difference $\Delta H_{(total)}$ on a scale of 0 to 1. Here we can say that enthalpy relaxes into the equilibrium supercooled liquid state because no crystal nuclei are formed on the time scale of experimental observation. The fitted curve yields relaxation time τ of 317 sec and stretched exponential function β of 0.88.

Four examples of isothermal enthalpy relaxation fitted with stretched exponential

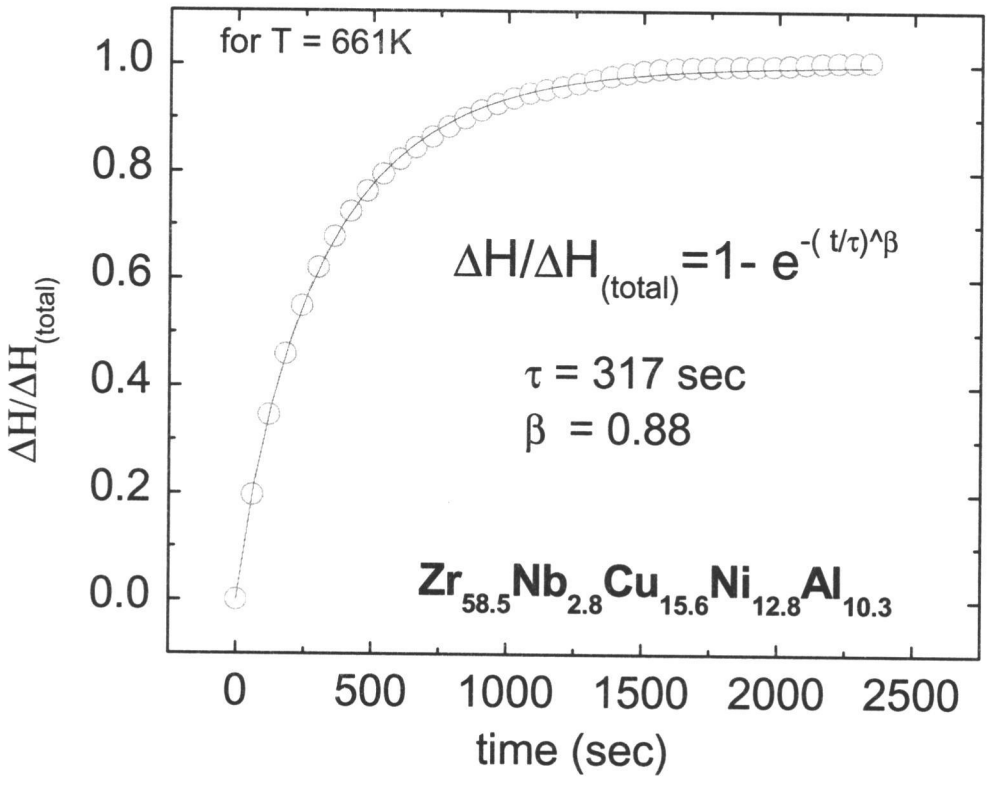

Figure 22 Illustration of curve fitting with stretched exponential function for temperature of 661 K that yields stretching exponent β of 0.88 and relaxation time τ of 317 sec.

function for $Zr_{58.5}Cu_{15.6}Ni_{12.8}Al_{10.3}Nb_{2.8}$ are plotted in Fig. 23. It is seen from the plot that the enthalpy is increasing towards temperature away from the glass transition temperature e.g 633 K. At the same time a longer time for relaxation is observed which is contributed to slow relaxation kinetics and large initial departure from equilibrium far from the glass transition temperature. On the contrary, gradual decrease in relaxation time and thus enthalpy towards the glass transition temperature e.g. 663 K are observed due to rapid crystallization kinetics and small initial departure from equilibrium. This implies that the area under the curve increases as the relaxation time increases. Apparent decrease in stretching exponent β at lower temperatures further helps in deciding behavior of amorphous material far from the glass transition temperature.Variation of stretching exponent β with isothermal temperature is shown in Fig. 24. As shown here, the stretching exponent β is close to 0.79 far from the glass transition temperature and increases linearly with increase in isothermal temperature and in the vicinity of the glass transition temperature. This indicates strong liquid behavior of $Zr_{58.5}Cu_{15.6}Ni_{12.8}Al_{10.3}Nb_{2.8}$, which is in contrast to typical fragile liquid having stretching exponent below 0.5 at the glass transition.[10]

In the kinetic relaxation experiments it is found that enthalpy relaxation does not follow the VFT relation. Instead it is best fitted by Arrhenius relation on a plot of relaxation time τ as a function of inverse temperature (1000/T) as shown in Fig. 25. Arrhenius relation in terms of relaxation time is given by

$$\tau = \tau_0 \cdot \exp\left(\frac{Q}{RT}\right) \tag{31}$$

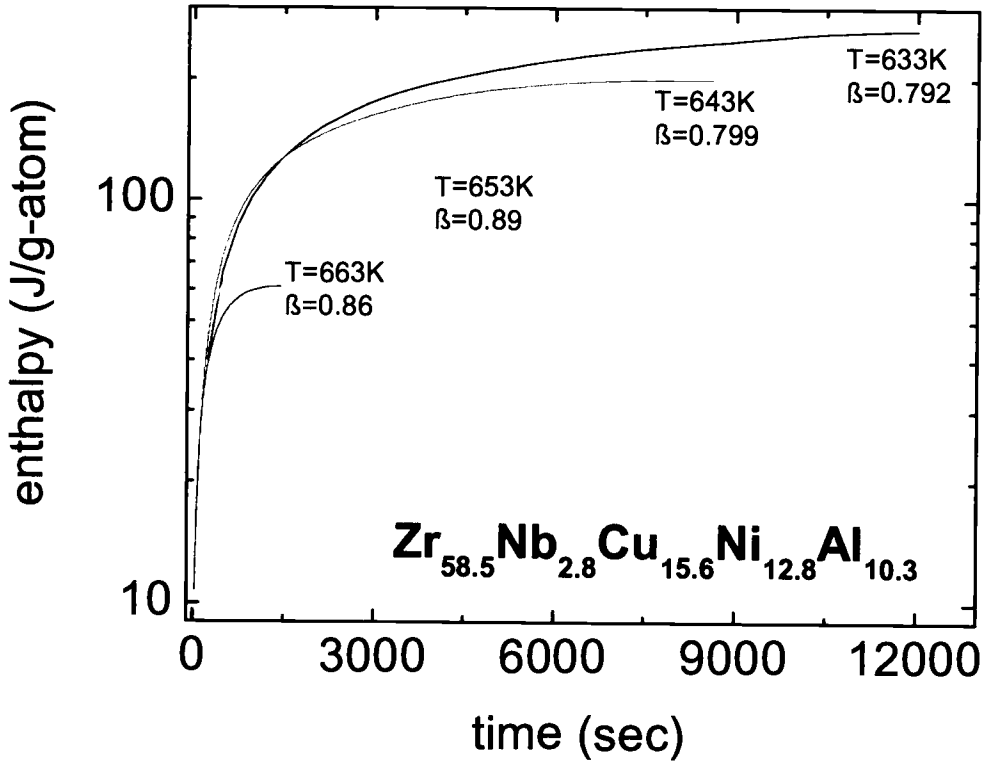

Figure 23 Isothermal enthalpy relaxation measurement as a function of time for four different temperatures. Stretched exponential function is used for fitting data.

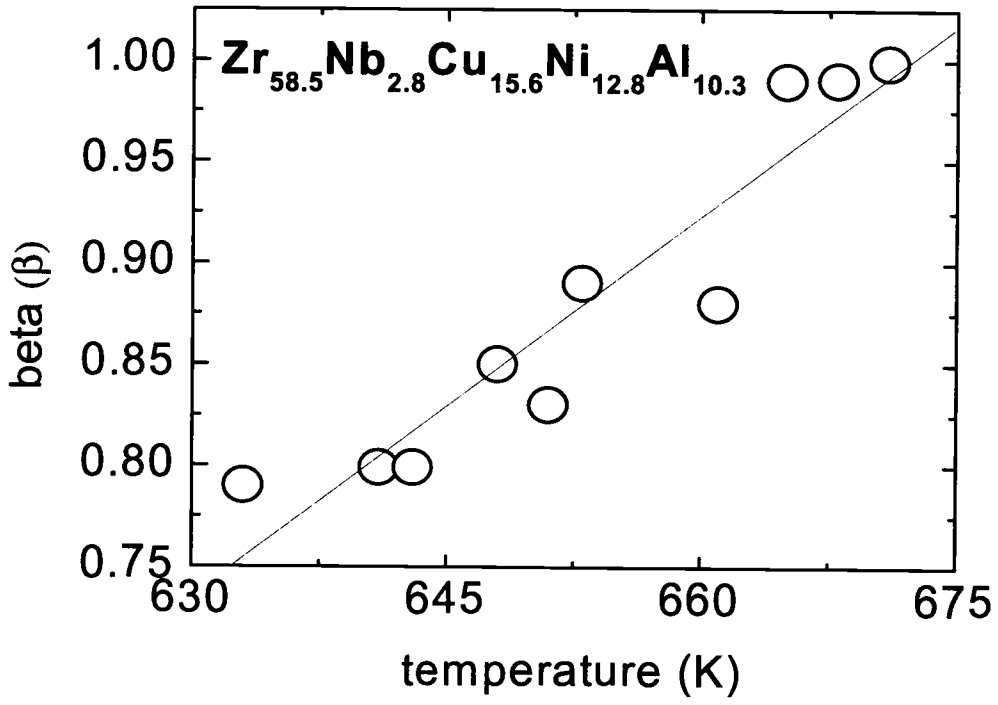

Figure 24 Change in stretching exponent β with isothermal annealing temperature. Data points are fitted with linear fit.

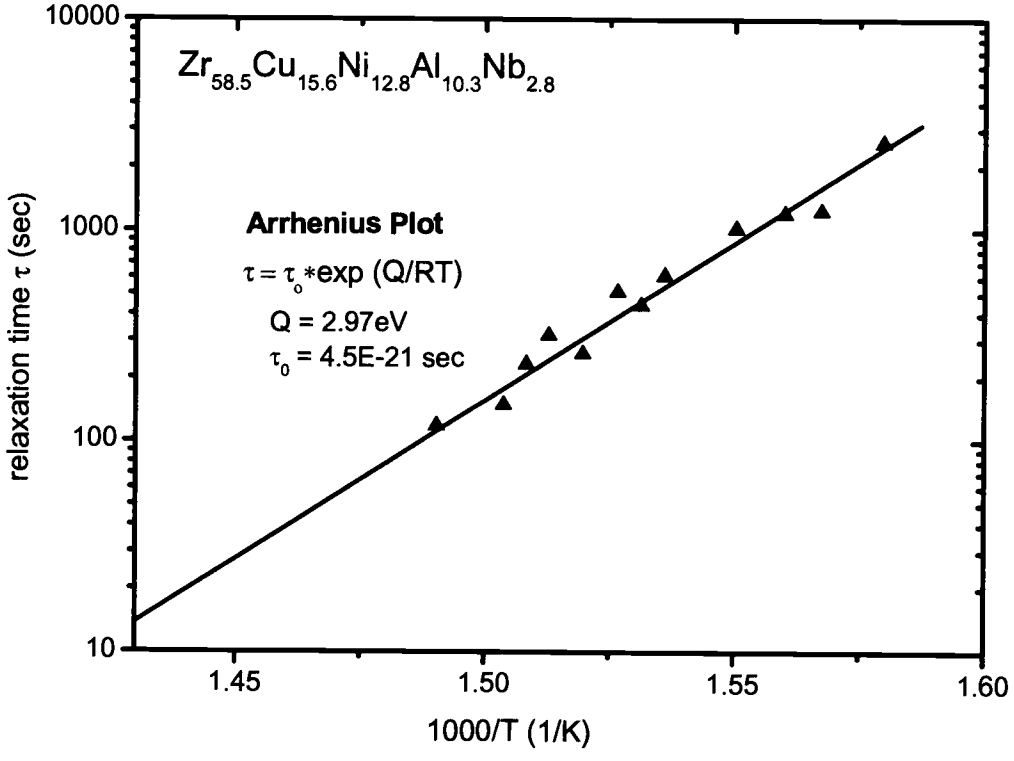

Figure 25 Arrhenius plot of the relaxation time of $Zr_{58.5}Cu_{15.6}Ni_{12.8}Al_{10.3}Nb_{2.8}$ as a function of inverse temperature. Fitting data with the Arrhenius relation yields activation energy Q of 2.97 eV and pre-exponential constant τ_0 of 4.5E-21 sec.

where, τ_0 is a pre-exponential constant, R is the gas constant, Q is the activation energy and T the absolute temperature. The fitted curve yields $\tau_0 = 4.5 \times 10^{-21}$ sec and activation energy Q of 2.97 eV.

4.2.3 Crystallization Kinetics

During our experiments isothermal crystallization is observed on annealing $Zr_{58.5}Cu_{15.6}Ni_{12.8}Al_{10.3}Nb_{2.8}$ in the glass transition region. Zhuang and Wang[58] observed that crystallization by annealing the alloy near T_g or in the supercooled liquid region are mainly due to apparent decrease in activation energy of crystallization compared to that of the glass transition. Typical crystallization behavior of the melt is indicated by exothermic heat release upon crystallization of the metastable supercooled liquid. Three such isothermal crystallization curves obtained in the temperature range between 713 K and 753 K at 20 K interval are shown in Fig. 26. With isothermal annealing at a temperature far from the glass transition temperature i.e. near 753 K, single and sharp crystallization peak is observed with less time for initiation of crystallization because at higher temperatures the kinetics is relatively faster. Crystallization kinetics slows down toward the vicinity of the glass transition temperature, which results in progressive broadening of the crystallization peak. Isothermal heating above 713 K yields two isothermal crystallization peaks, which is possibly due to liquid-liquid immiscibility or phase separation that further proves slow kinetics near T_g. It is reported in literature that phase separation is observed as a result of chemical short-range order in BMG forming liquid.[10]

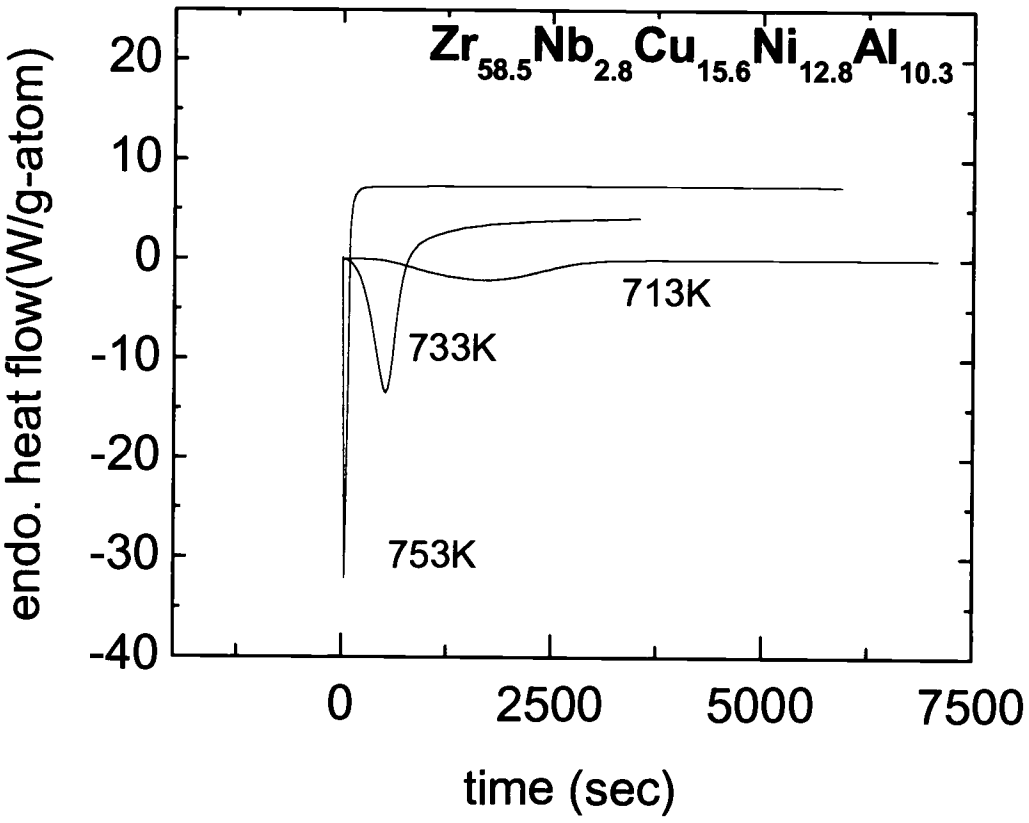

Figure 26 DSC scans of isothermal crystallization behavior for various temperatures. Single peak is observed for temperatures in the vicinity of glass transition while at temperature above 713 K two distinct exothermic peak is perceived.

An isothermal TTT diagram was constructed by plotting results of the isothermal crystallization experiments carried out at various temperatures in the glass transition and the supercooled liquid region. In this TTT diagram onset, peak and end time of crystallization is detected during isothermal annealing and is plotted as a function of temperature as shown in Fig. 27. Here, as shown in figure, two distinct crystallization peaks with onset, peak and end time are observed in proximity to glass transition temperature. The curve obtained follows the lower half of the typical C-shape curve as expected for a TTT diagram. Limitation of the DSC machine to go to higher temperatures restricts in getting complete C-shape of the diagram and thus getting critical heating rate of $Zr_{58.5}Cu_{15.6}Ni_{12.8}Al_{10.3}Nb_{2.8}$ in this experiment.

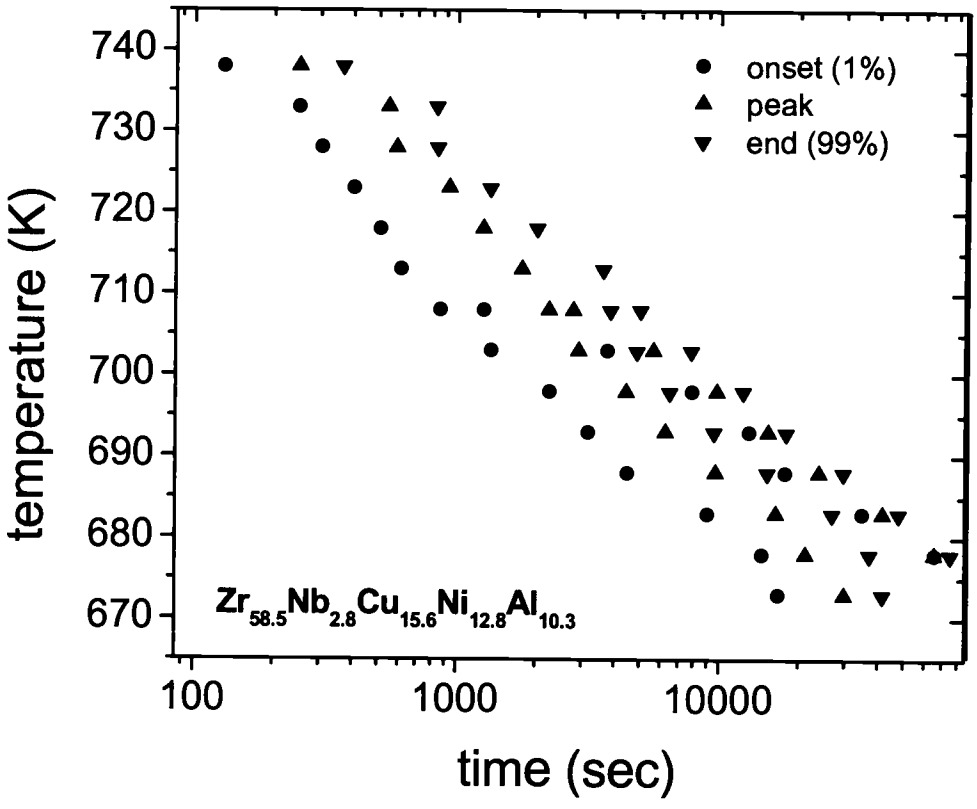

Figure 27 Time Temperature Transformation (TTT) diagram constructed from the isothermal crystallization experiment. Plot shows the onset, peak and end of crystallization event.

5 DISCUSSION

5.1 Thermodynamics

The thermodynamic study mainly involves determining the thermodynamic functions and monitoring change in these functions with temperature. In this research specific heat capacity measurement of $Zr_{58.5}Cu_{15.6}Ni_{12.8}Al_{10.3}Nb_{2.8}$ was done using sapphire as a reference. By measuring the specific heat in glassy, supercooled liquid and crystalline regions as shown in Fig. 15, it is possible to calculate change in enthalpy, entropy and Gibbs free energy between liquid and crystalline state as a function of temperature using Equation 21, 22 and 24. The enthalpy difference between liquid and crystalline state at T_g represents the frozen-in enthalpy. In addition, enthalpy and entropy of fusion were calculated from DTA experiments by calculating the area under the melting peak. The Kauzmann temperature T_k is believed to be the lowest temperature at which a supercooled liquid can exist without crystallizing or forming a glass.[59] Table 1 gives the enthalpy and entropy of fusion along with Kauzmann temperature, melting temperature and onset glass transition temperature for a heating rate of 0.33 K/s for $Zr_{58.5}Cu_{15.6}Ni_{12.8}Al_{10.3}Nb_{2.8}$.

BMG alloy	T_k (K)	T_g (K)	T_f (K)	ΔH_f (kJ/g-atom)	ΔS_f (J/g-atom K)
$Zr_{58.5}Cu_{15.6}Ni_{12.8}Al_{10.3}Nb_{2.8}$	645	660	1110	8.68	7.82

Table 1 Tabulated value of Kauzmann, glass transition and melting temperature along with enthalpy and entropy of fusion of $Zr_{58.5}Cu_{15.6}Ni_{12.8}Al_{10.3}Nb_{2.8}$ in appropriate units.

It is seen from the calculations that smaller enthalpy and entropy difference between the liquid and crystalline state results in smaller Gibbs free energy difference which is indicative of good glass forming ability of this multicomponent alloy from a thermodynamic point of view. In general, glassy material with a smaller critical cooling rate shows smaller Gibbs free energy difference between liquid and crystalline state compared to material with higher critical cooling rate.[51] The origin of this smaller Gibbs free energy difference lies in small entropy of fusion. At the melting point the entropy of fusion determines the slope of the Gibbs free energy curve. The smaller the slope, the smaller the free energy difference at the melting point which results in small driving forces for crystallization. The origin for the small enthalpy and entropy of fusion are likely the small free volume and the tendency to form chemical short-range order at the melting point. Comparison of $Zr_{58.5}Cu_{15.6}Ni_{12.8}Al_{10.3}Nb_{2.8}$ with other glass forming alloys,[60] as shown in Fig. 28, reveals the smaller Gibbs free energy of this system.

Turnbull's qualitative criterion[24] of reduced glass transition temperature T_{rg}, ratio of glass

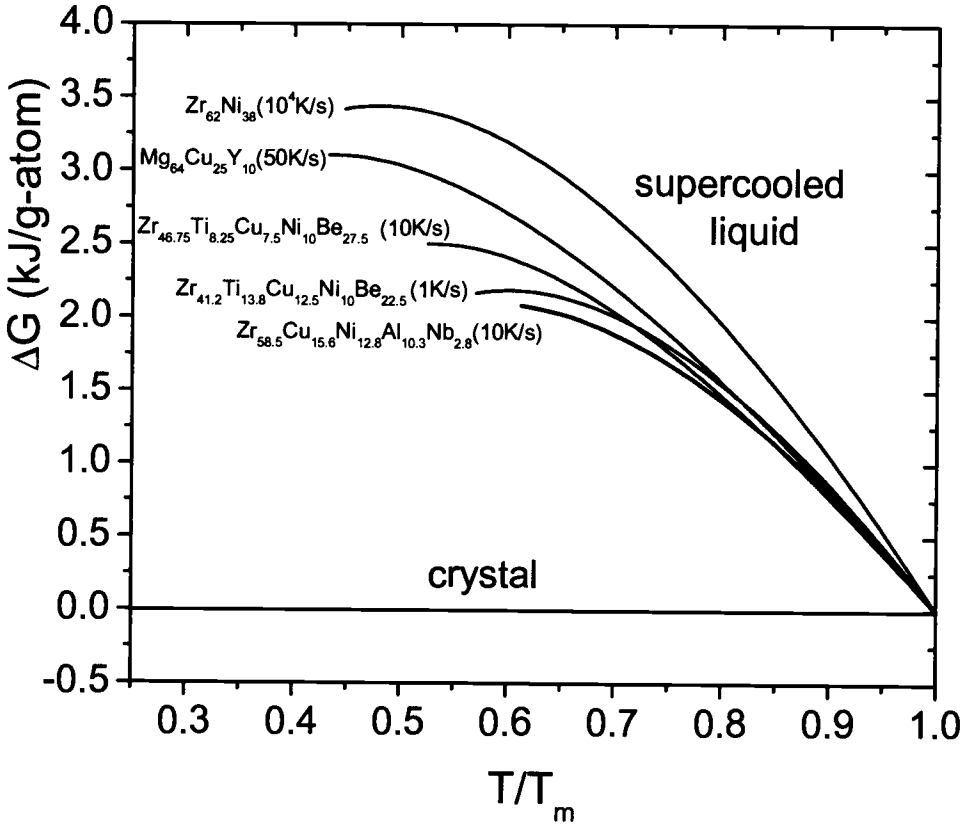

Figure 28 Difference in Gibbs free energy of the supercooled liquid with respect to the crystal for various glass forming alloys.

transition temperature to liquidus temperature, demonstrates that higher T_{rg} is manifested by sluggish crystallization kinetics and hence high glass forming ability of the alloy. He also suggested that regardless of the type of glass forming alloy, it exhibits a T_{rg} value close to 0.66,[29] if the critical cooling rate is close to 1 K/s. Though $Zr_{58.5}Cu_{15.6}Ni_{12.8}Al_{10.3}Nb_{2.8}$ can be prepared by critical cooling rate of 1.75 K/s, the value of T_{rg} is found to be less than 0.6 in our experiments that contradicts Turnbull's criteria[24] or in other words it fails in justifying the good glass forming ability of this alloy. But, there is no disagreement with the concept of the large Supercooled Liquid Region (SLR width) as suggested by Inoue.[27] A comparatively high SLR width, ΔT=94 K, of $Zr_{58.5}Cu_{15.6}Ni_{12.8}Al_{10.3}Nb_{2.8}$ leads to high resistance to crystallization.

One of the criteria in formation of bulk metallic glass requires that its composition should be close to deep eutectic and should have lower melting temperature. $Zr_{58.5}Cu_{15.6}Ni_{12.8}Al_{10.3}Nb_{2.8}$ is found to have lowest melting temperature in comparison to alloys in its neighboring composition.[9]

5.2 Kinetics

5.2.1 Heating Rate Kinetics

Fragility of the glass reflects the heating rate dependence of the glass transition.[10] A small and large heating rate dependency is the characteristic of fragile and strong glass respectively. Angell's fragility concept[45] gives new insight for glass transition, structural relaxation phenomenon as well as structure of glass or supercooled liquid. In bulk metallic glass formers where the main bonding type is metallic, efforts have been made to

determine how closely the data of $Zr_{58.5}Cu_{15.6}Ni_{12.8}Al_{10.3}Nb_{2.8}$ follow the fragility concept. Fragility concept is a classification scheme used to describe different temperature dependencies of the viscosity or relaxation time. Fragility parameter $D=BT_0$ is also a measure of the structural strength of a glassy system. Where fragility parameter can run from 2 to as high as 100, D value of 19.7 signifies $Zr_{58.5}Cu_{15.6}Ni_{12.8}Al_{10.3}Nb_{2.8}$ as a strong glass former. It is also suggestive of sluggish crystallization kinetics near the glass transition region. Table 2 compares the fragility of $Zr_{58.5}Cu_{15.6}Ni_{12.8}Al_{10.3}Nb_{2.8}$ with other bulk metallic glass forming alloys.[61,62] There is a general tendency that the fragility parameter increases with the number of components.

Glass forming alloy	Fragility parameter D
$Zr_{58.5}Cu_{15.6}Ni_{12.8}Al_{10.3}Nb_{2.8}$	19.7
$Zr_{46.75}Ti_{8.8}Cu_{7.5}Ni_{10}Be_{27.5}$	22.7
$Zr_{41.2}Ti_{13.8}Cu_{13.5}Ni_{10}Be_{22.5}$	18.5
$Zr_{65}Al_{7.5}Cu_{17.5}Ni_{10}$	13.8
$Zr_{60}Al_{15}Ni_{25}$	11.6

Table 2 Comparison of fragility parameter D of $Zr_{58.5}Cu_{15.6}Ni_{12.8}Al_{10.3}Nb_{2.8}$ with other Zr-based bulk metallic glass forming alloy.

5.2.2 Relaxation Kinetics

Time dependent relaxation phenomenon is not only important for improving basic understanding of glass transition and transport phenomena but also essential for perceiving insight into technologically important properties such as damping, yield

strength, ductile-to-brittle transition temperature, fracture toughness and fatigue crack growth rate in various glassy materials.[63] It was found for $Zr_{41}Ti_{14}Cu_{12.5}Ni_{10}Be_{22.5}$ alloy that relaxed structure exhibits considerable different acoustic and mechanical properties compared to as prepared and crystalline alloy. In particular improved strength and ductility is observed.[30] Though it's a case of further investigation in case of $Zr_{58.5}Cu_{15.6}Ni_{12.8}Al_{10.3}Nb_{2.8}$, improvement in various properties by relaxation may explore significant engineering applications of BMG forming alloys. Supercooling the liquid in transformation range results in freezing of liquid structure before the liquid relaxes towards the equilibrium. In order to reach the thermal equilibrium state from this structurally arrested non-equilibrium state of liquid, annealing has been carried out in the transformation range. The amount of heat dissipated during this transition is a measure of enthalpy of the sample and this process is known as enthalpy relaxation. Enthalpy relaxation test is performed here at lower temperatures below the glass transition. Above this temperature relaxation is fast compared to the laboratory time scale and hence hard to record experimentally. According to the best of Author's knowledge, this is the first direct measurement of enthalpy relaxation time scale in a metallic glass. Importance of the enthalpy relaxation process lies in its ability to contribute in understanding the liquid structure and indirectly the glass forming ability of bulk metallic glass forming alloy. During viscosity measurement of $Zr_{46.75}Ti_{8.8}Cu_{7.5}Ni_{10}Be_{27.5}$ it is observed that isothermal experiments are the most suitable means of obtaining equilibrium viscosity and hence all the enthalpy relaxation measurements of $Zr_{58.5}Cu_{15.6}Ni_{12.8}Al_{10.3}Nb_{2.8}$ were performed isothermally. Viscosity and enthalpy relax into a metastable equilibrium state of the

supercooled liquid and not a glassy metastable equilibrium state.[10] In terms of free volume theory, annealing can reduce open volume regions, which are associated with the frozen-in structural state, and so does the excess free energy associated with it.

As measurement of c_p always involve temperature change or continuous heating, it is difficult to measure it in isothermal experiments where measurements are always performed at constant temperatures. Also, it is not possible to measure high specific heat of supercooled liquid directly at low temperatures on laboratory time scale.[51] Because in cp measurements, the time required for temperature change is in seconds compared to the 9much longer time scale required for enthalpy relaxation. As only fraction of enthalpy relaxed during this time period of c_p measurement, it's not a useful tool for studying isothermal enthalpy relaxation.

Residual enthalpy is frozen in as the liquid undergoes glass transition. Upon isothermal annealing below glass transition temperature, frozen enthalpy of amorphous glass relaxes into the equilibrium supercooled liquid state as shown in Fig. 29. The actual enthalpy relaxation data points below the glass transition temperature are shown along with the enthalpy change as a function of temperature obtained from the thermodynamic experiments. Increase in Enthalpy difference ΔH between the glass and the supercooled liquid with decrease in temperature is shown in the plot. Enthalpy relaxation is associated with the structural state of the material. Structural relaxation, which in most of the cases assumed to be due to molecular motion, may not be true. It could be due to motion of defects in the solid.

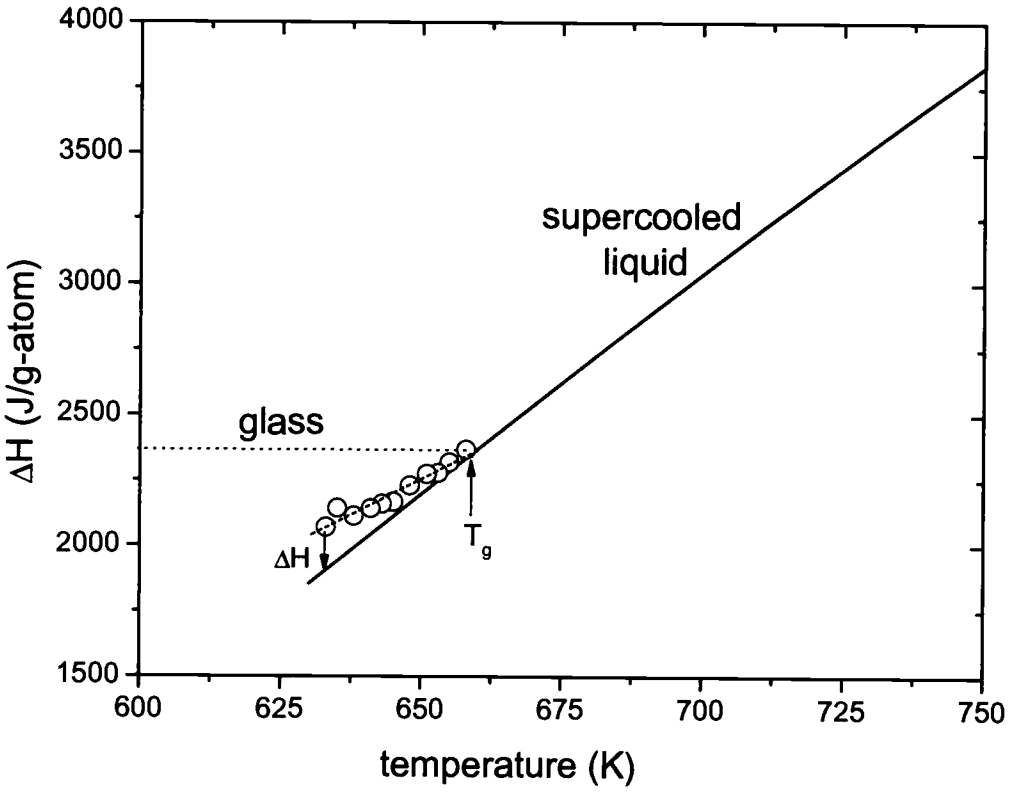

Figure 29 Enthalpy change between glass and supercooled liquid as a function of temperature for $Zr_{58.5}Cu_{15.6}Ni_{12.8}Al_{10.3}Nb_{2.8}$. (○) shows the actual data points from the enthalpy relaxation experiments below the glass transition temperature. Downward arrow indicates enthalpy difference ΔH between these two states.

In stretched exponential function Equation (29), stretching exponent β is a constant with $0 < \beta \leq 1$. It represents the width of the distribution of relaxation time. Where small value of β corresponds to broader distribution of relaxation time, its value close to 1 indicates its single exponentiality in relaxation function and also suggestive of predominance of single relaxation mechanism.[63]

For $Zr_{58.5}Cu_{15.6}Ni_{12.8}Al_{10.3}Nb_{2.8}$, Arrhenius expression describes the enthalpy relaxation time better than a VFT relation for isothermal relaxation experiments. Combined plot of Arrhenius fit, which is obtained by relaxation experiments, and VFT fit obtained from the heating rate experiments on a scale of relaxation time versus temperature is shown for comparison in Fig. 30. The time scale for the enthalpy relaxation cannot be fitted by VFT. It rather follows the time scale for diffusive processes. Considering this diffusive process in terms of atomic motion, reported by Suh and Dauskardt[35], by doing an experiment on Zr-Ti-Cu-Ni-Be bulk metallic glass that at higher temperatures above T_g, relaxation time scales are associated with the large-scale cooperative motion of groups of atoms. Instead at lower temperatures in proximity of T_g, relaxation can be well described by the local adjustment in atomic positions and not by the collective motion or changes in chemical order. The local adjustments in atomic positions which are described by the collective hopping mechanism, is likely to control the diffusion of medium sized (Al, Nb) and small sized (Cu, Ni) atoms in our BMG alloy. It was reported for $Zr_{41.2}Ti_{13.8}Cu_{12.5}Ni_{10}Be_{22.5}$ that medium sized atom such as Ni is likely to diffuse by collective hopping mechanism and smallest atom of Be by thermally activated jumps in

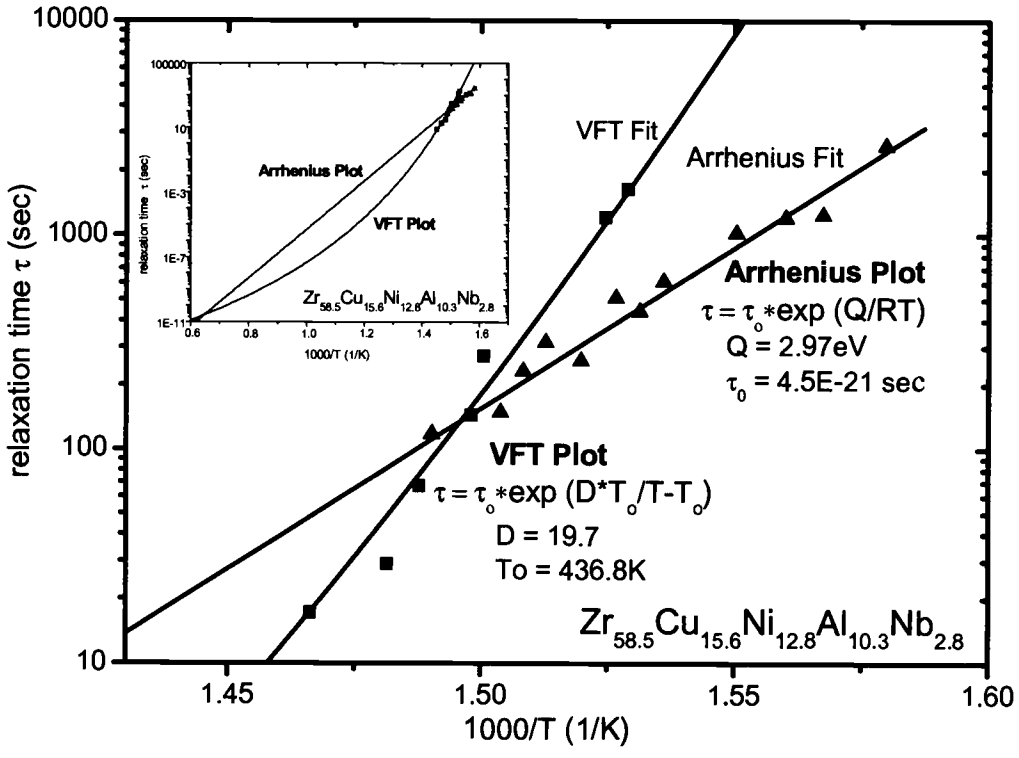

Figure 30 Combined plot of Arrhenius fit (▲) and VFT fit (■) for relaxation time as a function of inverse temperature. Inset picture shows the extrapolation of both curves to a very low value of relaxation time τ.

the deeply supercooled liquid state.[64] The collective hopping mechanism for medium sized atom such as Co is confirmed by isotope effect measurements in case of $Zr_{58.5}Cu_{15.6}Ni_{12.8}Al_{10.3}Nb_{2.8}$.[65] Activation energy obtained by fitting the enthalpy relaxation data is analogous to the activation energy of aluminum at lower temperatures which makes us believe that solid state diffusion at lower temperatures is mainly governed by the activated jumps of medium sized Al and Nb atoms. Yet, further experiments including quasielastic neutron scattering is essential to confirm these results.

5.2.3 Crystallization Kinetics

Two crystallization events observed in proximity of glass transition temperature, as shown in Fig. 28, represents that solubility and diffusivity decreases close to glass transition temperature and two independent nucleation mechanisms are active at that temperatures. Along with our TTT diagram, TTT diagram constructed by Hays et. al.[9] for $Zr_{58.5}Cu_{15.6}Ni_{12.8}Al_{10.3}Nb_{2.8}$ alloy by cooling the stable melt from liquidus temperature to isothermal temperature between the liquidus and glass transition temperature is shown in Fig. 31. Surprisingly lower half of TTT curve constructed from his experimental data is in continuous agreement with that of our data, which is obtained by heating from the amorphous state. In case of $Zr_{41.2}Ti_{13.8}Cu_{13.5}Ni_{10}Be_{22.5}$[66] and $Pd_{40}Ni_{40}P_{20}$[67] difference in crystallization behavior was observed between cooling from the stable melt and heating the amorphous sample and it was attributed to different growth rates experienced by crystalline nuclei. No difference in crystallization mechanism while heating from the amorphous state or cooling from the stable melt indicates that $Zr_{58.5}Cu_{15.6}Ni_{12.8}Al_{10.3}Nb_{2.8}$

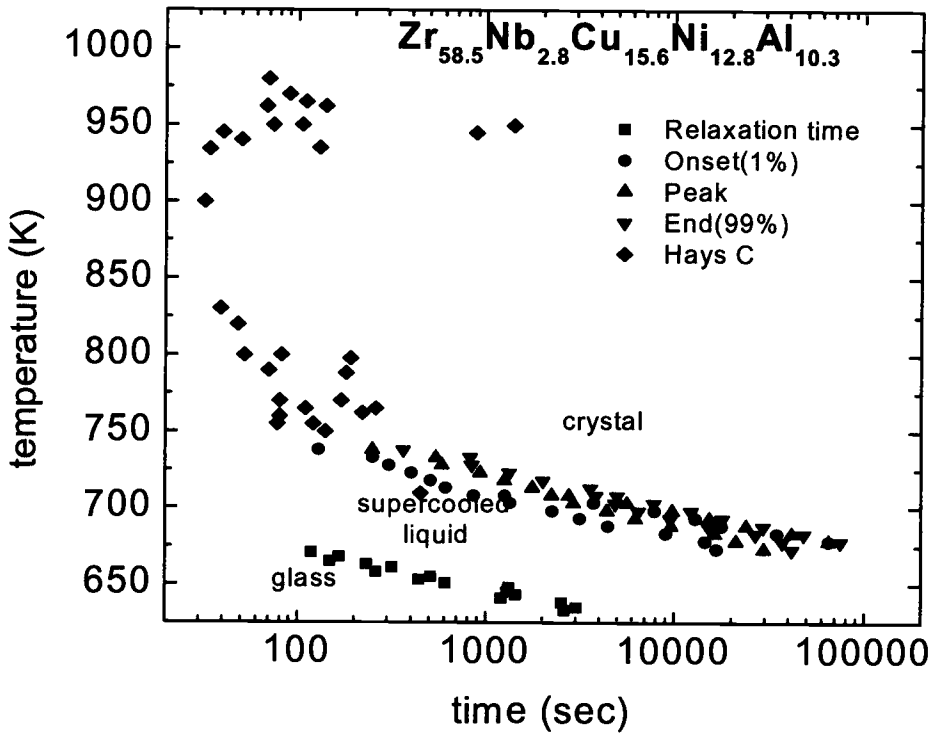

Figure 31 By plotting isothermal TTT diagram for onset, peak and end of crystallization along with relaxation data, three different domains are distinguished called crystal, supercooled liquid and glass. Data plotted by C.C.Hays for isothermal temperature by cooling the $Zr_{58.5}Cu_{15.6}Ni_{12.8}Al_{10.3}Nb_{2.8}$ from liquidus temperature is in good agreement with our experimental data.

glass forming liquid is stable and homogeneous at all temperatures and follows the regular nucleation and growth mechanism. Furthermore, by plotting the data of isothermal experiments in terms of enthalpy relaxation time (square black dots) in the same TTT plot, it falls just below and in the same line of the crystallization data. As the sample relaxes from glassy state to the supercooled liquid state in the lower temperature region, plotting the relaxation data separates it into two regions, which are on either side of glass transition region. The lower temperature region depicts the initial glassy state of the sample, which is followed by supercooled liquid region at comparatively higher temperatures. Eventually material crystallizes on isothermally heating above the glass transition temperature and so region beyond the right hand side of these crystalline data points is known as crystalline region. In conclusion, three dissimilar regions namely crystal, supercooled liquid and glass are clearly distinguished in TTT plot.

6 CONCLUSION

The thermodynamic and kinetic behavior of $Zr_{58.5}Cu_{15.6}Ni_{12.8}Al_{10.3}Nb_{2.8}$ bulk metallic glass forming alloy was studied using Differential Scanning Calorimetry (DSC) and Differential Thermal Analysis (DTA) techniques. To calculate the thermodynamic functions, specific heat capacity measurements were carried out in the glass region, supercooled liquid region and crystalline region with reference to sapphire. Heats of fusion of this alloy were calculated from DTA scans. Difference in the Gibbs free energy between the liquid and the crystalline state were calculated by taking into account the enthalpy and entropy differences. Small Gibbs free energy difference between liquid and crystalline state is indicative of smaller driving force for crystallization, which leads to likelihood of good glass forming ability of this alloy.

Kinetics of $Zr_{58.5}Cu_{15.6}Ni_{12.8}Al_{10.3}Nb_{2.8}$ was studied by heating rate as well as isothermal experiments. The heating rate dependence of the glass transition reflects the fragility of the material.[10] Heating rate experiments were performed between 8.33×10^{-3} and 3.33 K/s. Plot of relaxation time as a function of inverse temperature is used to calculate the fragility parameter D and VFT temperature T_o using VFT equation. High fragility parameter of this alloy is indicative of its strong liquid nature.

Isothermal relaxation and crystallization kinetics were studied in the vicinity of the glass transition region. An experimental method developed for the enthalpy relaxation experiments that were carried out below the glass transition temperature is used to evaluate the relaxation time τ and stretching exponent β using stretched exponential

function. The value of stretching exponent β is close to 0.8 in the proximity of glass transition temperature and increases with increase in isothermal temperature. This large value of stretching exponent also reflects the strong liquid nature of this alloy. The relaxation time τ obtained by fitting the stretched exponential relation is plotted as a function of isothermal temperature and is best fitted with the Arrhenius equation. Best fit obtained with Arrhenius relation instead of VFT suggests that enthalpy relaxation is controlled by the solid-state diffusion in this alloy. The activation energy of 2.97 eV was compared with the activation energy of constituent metallic elements and it is believed that motion of the medium and smaller sized atoms of this alloy, which are likely to diffuse by the collective hopping mechanism, govern the relaxation in the proximity of glass transition temperature.

The lower half of the Time Temperature Transformation (TTT) diagram constructed from the isothermal crystallization experiment follows the typical C-shape of the curve and two crystallization peaks obtained close to glass transition reflect the sluggish crystallization kinetics. TTT diagram constructed by C. C. Hays[9] on cooling the sample from the stable melt to the isothermal temperature is compared with our TTT diagram, which is obtained by heating the sample from lower temperature to the isothermal temperature. Continuous agreement between these two TTT plot indicates that this alloy is more stable and homogeneous over the entire temperature range and it follows the regular nucleation and growth mechanism regardless of heating and cooling effect.

In order to further validate the $Zr_{58.5}Cu_{15.6}Ni_{12.8}Al_{10.3}Nb_{2.8}$ bulk metallic glass forming alloy's strong liquid behavior in the glass transition region, viscosity measurements could

be performed. Inelastic neutron scattering technique can be used in further study of relatively slow relaxation dynamics of $Zr_{58.5}Cu_{15.6}Ni_{12.8}Al_{10.3}Nb_{2.8}$ glass forming alloy.

REFERENCES

1 http://easy.stanford.edu/dauskardt/kathy_flores/BMG/bmg.html, 28 June (2003).

2 Klement W., Willens R. H., and Duwez P. 1960, "The formation of non-crystalline Au-Si alloys by rapid quenching", Nature, 187 (1960), 869.

3 J. Jackle, "Models of the glass transition", Rep. Prog. Phys., 49 (1986), 171.

4 William L. Johnson, "Bulk Glass-Forming Metallic Alloys: Science and Technology", MRS Bulletin, (1999), 42.

5 A. Inoue, T. Zhang and T. Masumoto, "Zr-Al-Ni amorphous-alloys with high glass-transition temperature and significant supercooled liquid region", Materials Transaction, JIM 31 (1990), 177.

6 A. Peker and W. L. Johnson, "A highly processable metallic glass – $Zr_{41.2}Ti_{13.8}Cu_{12.5}Ni_{10.0}Be_{22.5}$", Applied Physics Letters, 63 (1993), 2342.

7 N. Nishiyama and A. Inoue, Glass-forming ability of bulk $Pd_{40}Ni_{10}Cu_{30}P_{20}$ alloy", Materials Transactions, JIM 37 (1996), 1531.

8 C. C. Hays, J. Schroers, U. Geyer, S. Bossuyt, N. Stein and W. L. Johnson, "Glass Forming Ability in the Zr-Nb-Ni-Cu-Al Bulk Metallic Glasses", Materials Science Forum, 343-346 (2000), 103.

9 C. C. Hays, J. Schroers, T. J. Rathz, R. W. Hyers, J. R. Rogers and Robinson and W. L. Johnson, "Vitrification and Determination of the Crystallization Time Scales of the Bulk-Metallic-Glass-Forming Liquid $Zr_{58.5}Nb_{2.8}Cu_{15.6}Ni_{12.8}Al_{10.3}$", Applied Physics Letters, 79 (2001), 1605.

10 R. Busch, E. Bakke and W. L. Johnson, "Viscosity of the supercooled liquid and relaxation at the glass transition of the $Zr_{46.75}Ti_{8.25}Cu_{7.5}Ni_{10}Be_{27.5}$ bulk metallic glass forming alloy", Acta Materialia, 46 (1998), 4725.

11 R. Bohmer, K. L. Ngai, C. A. Angell, D. J. Plazek, "Nonexponential relaxations in strong and fragile glass formers", Journal of Chemical Physics, 99 (1993), 4201.

12 C. A. Angell, "Relaxation in liquids, polymers and plastic crystals – strong/fragile patterns and problems", Journal of Non-Crystalline Solids, 131-133 (1991), 13.

13 T. A. Waniuk, R. Busch, A. Masuhr and W. L. Johnson, "Equilibrium viscosity of the $Zr_{41.2}Ti_{13.8}Cu_{12.5}Ni_{10}Be_{22.5}$ bulk metallic glass-forming liquid and viscous flow

during relaxation, phase separation and primary crystallization", Acta Materialia, 46 (1998), 5229.

14 P. Duwez, Metallic Glasses, Papers presented at a seminar of the Materials Science Division of the American Society for Metals, Ohio, Sept 18 and 19, 158, (1976).

15 http://www.lbl.gov/Ritchie/Programs/METGLASS/, 2 July (2003).

16 http://www.arofe.army.mil/Conferences/BMG/BMG_TBL8.pdf, 8 July (2003).

17 Akihisa Inoue, "Stabilization of Metallic Supercooled Liquid and Bulk Amorphous Alloys", Acta Materialia, 48 (2000), 279.

18 http://www.jpl.nasa.gov/releases/2000/genesiscollector.html, 10 July (2003).

19 D. A. Porter and K. E. Easterling, "Phase Transformations in Metals and Alloys", 2nd Edition, 1992, 2.

20 M. D. Ediger, C. A. Angell, Sidney R. Nagel, "Supercooled Liquids and Glasses", The Journal of Physical Chemistry, 100 (1996), 13200.

21 Class notes from "Amorphous Materials", 2003.

22 Ralf Busch, "The Thermophysical Properties of Bulk Metallic Glass-Forming Liquids", JOM, 52 (2000), 39.

23 Chen H. S. and Turnbull D., "Formation, stability and structure of palladium-silicon based alloy glasses", Acta Metallurgica, 17 (1969), 1021.

24 D. Turnbull and J. C. Fisher, "Rate of nucleation in condensed systems", Journal of Chemical Physics, 17 (1949), 71.

25 Peker A., and Johnson W. L., "A Highly Processable Metallic Glass: $Zr_{41.2}Ti_{13.8}Cu_{12.5}Ni_{10.0}Be_{22.5}$", Applied Physics Letters, 63 (1993), 2342.

26 Inoue A, Mater Trans, "High-strength bulk amorphous-alloys with low critical cooling rates", Japan Inst. Metals, 36 (1995), 866.

27 H. Lee, Y. Qi, A. Strachan, T. Cagin, W. Johnson, Goddard III, MRS Proceedings, 644 (2000).

28 Beaker R. and Döring W., Ann. Phy. LPZ., 24 (1935), 719.

29 Turnbull D., "Under what conditions can a glass be formed", Contemporary Physics, 10 (1969), 473.

30 Uhlmann D. R., Journal of Non-Crystalline Solids, 7 (1972), 337.

31 Gong Li, Limin Wang, Zaiji Zhan, Liling Sun, Jun Zhang and Wenkui Wang, "The Influence of Structural Relaxation on the Mechanical Properties of $Zr_{41}Ti_{14}Cu_{12.5}Ni_{10}Be_{22.5}$ Bulk Metallic Glass", Journal of Physics, 14 (2002), 11077.

32 Cohen M. H. and Turnbull D., "Molecular transport in liquids and glasses", Journal of Chemical Physics, 31 (1959), 1164.

33 A. Masuhr, R. Busch, W. L. Johnson, "Thermodynamics and kinetics of the Zr41.2Ti13.8Cu10.0Ni12.5Be22.5 bulk metallic glass forming liquid: glass formation from a strong", Journal of Non-Crystalline Solids, 250-252 (1999), 566.

34 G. S. Grest, M. H. Cohen, Adv. Chem. Phys. 48 (1981), 455.

35 M. L. William, R. F. Landel, J. D. Ferry, J.am. Chem. Soc., 77 (1955), 3701.

36 Daewoong Suh, Reinhold H. Dauskardt, "Effects of Open-Volume Regions on Relaxation Time Scales and Fracture Behavior of a Zr-Ti-Ni-Cu-Be Bulk Metallic Glass", Journal of Non-Crystalline Solids, 317 (2003), 181.

37 W. Kauzmann, "Thermodynamics of liquids at large undercoolings", Chemical Review, 43 (1948), 219.

38 G. Adam and J. H. Gibbs, "On temperature dependence of cooperative relaxation properties in glass-forming liquids", Journal of Chemical Physics, 43 (1965), 139.

39 J. H. Gibbs and E. A. Di. Marzio, "Nature of the glass transition and the glassy state", Journal of Chemical Physics, 28 (1958), 373.

40 Nelson D. R., "Order, frustration, and defects in liquids and glasses", Physical Review, B 28 (1983), 5515.

41 Kohlrausch R., Pogg. Ann. Phys., 156 (1854), 179.

42 Williams G and Watts D. C., "Non-symmetrical dielectric relaxation behavior arising from a simple empirical decay function", Transactions of the Faraday Society, 66 (1970), 80.

43 Johari G. P., Goldstei M., "Viscous liquids and glass transition .3. secondary relaxations in aliphatic alcohols and other nonrigid molecules", Journal Chemical Physics, 53 (1970), 2372, 55 (1971), 4245.

44 Greet R. J. and Magil J. H., "An empirical corresponding-states relationship for liquid viscosity", Journal of Physical Chemistry, 71 (1967), 1746.

45 Angell C. A., "Formation of glasses from liquids and biopolymers", Science, 267 (1995), 1924.

46 Nemilov S. V., "Correlation of crystallization character of glass melts with the temperature-dependence of their viscosity and the degree of spatial structural connectiveness", Glass Physics and Chemistry, 21 (1995), 91.

47 Phillips J. C., "Stretched exponential relaxation in molecular and electronic glasses", Reports on Progress in Physics, 59 (1996), 1133.

48 Jan Schroers, Ralf Busch and William L. Johnson, "Crystallization Kinetics of the Bulk-glass-forming $Pd_{43}Ni_{10}Cu_{27}P_{20}$ Melt", Applied Physics Letters, 77 (2000), 1158.

49 http://las.perkinelmer.com/home.htm, 12 July (2003).

50 http://wwwswt.informatik.unirostock.de/englisch/projekte/Physik2000/ExperimentII /ta2web001.pdf, 15 July (2003).

51 Pieter Tuinstra, Peter A. Duine, jilt Sietsma, and A.van den Beukel, "The Calorimetric Glass Transition of Amorphous $Pd_{40}Ni_{40}P_{20}$", Acta Metallurgica Materialia 43(1995), 2815.

52 Busch and W. L. Johnson, "The Kinetic glass transition of the $Zr_{46.75}Ti_{8.25}Cu_{7.5}Ni_{10}Be_{27.5}$ bulk metallic glass former-supercooled liquids on a long time scale", Applied Physics Letters, 72 (1998), 2695.

53 R. Busch, W. Liu, and W. L. Johnson, "Thermodynamics and kinetics of the $Mg_{65}Cu_{25}Y_{10}$ bulk metallic glass forming liquid", Journal of Applied Physics, 83 (1998), 4134.

54 Jan Schroers, William L. Johnson and Ralf Busch, "Repeated Crystallization in Undercooled $Zr_{41}Ti_{14}Cu_{12.}Ni_{10}Be_{23}$ Liquids, Applied Physics Letters, 76 (2000), 2343.

55 http://www.jhu.edu/~matsci/people/faculty/hufnagel/hufnagel.html, July 30, 2003.

56 O. Kubaschewski, C. B. Alcock and P. J. Spencer, "Materials Thermochemistry", 6^{th} ed., Pergamon, New York, 1993.

57 Bruning R. and Samwer K., " Glass-transition on long-time scales", Physical Review B, 46 (1992), 11318.

58 Yan Xin Zhuang and Wei Hua Wang, "Effects of relaxation on glass transition and crystallization of ZrTiCuNiBe bulk metallic glass", Journal of Applied Physics, 87 (11) (2000), 8209.

59 S. C. Glade, R. Busch, D. S. Lee, W. L. Johnson and R. K. Wunderlich and H. J. Fecht, "Thermodynamics of $Cu_{47}Ti_{34}Zr_{11}Ni_{14.6}Al_{10}Ti_5$ and $Zr_{57}Cu_{15.4}Ni_{12.6}Al_{10}Nb_5$ bulk metallic glass forming alloys", Journal of Applied Physics, 87 (10) (2000), 7242.

60 R. Busch, A. Masuhr, W. L. Johnson, "Thermodynamics and kinetics of Zr-Ti-Cu-Ni-Be bulk metallic glass forming liquids", Materials Science and Engineering, A304-306 (2001), 97.

61 Lu L. R., Wilde G., Gorler G. P., Fecht H. J. and Willnecker R., "Investigation of specific heat and thermal expansion in the glass-transition regime of Pd-based metallic glasses", Journal of Non-Crystalline Solids, 274 (2000), 294.

62 Loffler J. F., Bossuyt S., Glade S. C., Johnson W. L., Wanger W. and Thiyagurajon, "Crystallization of bulk amorphous Zr-Ti (Nb)-Cu-Ni-Al", Applied Physics Letters, 77 (2000), 525.

63 Daewoong Suh and Reinhold H. Dauskardt, "Mechanical relaxation time scales in a Zr-Ti-Ni-Cu-Be bulk metallic glass", Journal of Materials Research, 17 (2002), 1254.

64 A. Masuhr, T. A. Waniuk, R. Busch, and W. L. Johnson, "Time scales for viscous flow, atomic transport, and crystallization in the liquid and supercooled liquid states of $Zr_{41.2}Ti_{13.8}Cu_{12.5}Ni_{10}Be_{22.5}$", Physical Review Letters, 82 (1999), 2290.

65 H. Ehmler, A. Heesemann, K. Rätzke, F.Faupel, U. Geyer, "Mass dependence of diffusion in a supercooled metallic melt", Physical Review Letters, 80 (1998), 4919.

66 Jan Schroers, Andreas Masuhr, William L. Johnson and Ralf Busch, "Pronounced asymmetry in the crystallization behavior during constant heating and cooling of a bulk metallic glass-forming liquid", Physical Review B, 60 (1999), 11855.

67 H. W. Kui and D. Turnbull, "Melting of $Ni_{40}PD_{40}P_{20}$ Glass", Applied Physics Letter, 47 (1985), 796.